European Journal of Medicinal Chemistry 214 (2021) 113203

Contents lists available at ScienceDirect

European Journal of Medicinal Chemistry

journal homepage: http://www.elsevier.com/locate/ejmech

Synthesis and biological evaluation of novel *N*-substituted benzamides as anti-migration agents for treatment of osteosarcoma

Xiaojing Chen [a, 1], Guangbao Wang [a, 1], Ali Mohammed Mohammed Alsayed [a, 1], Zongxuan Du [a], Lu liu [a], Yue Ma [a], Peng Liu [a], Qianwen Zhang [a], Xianxin Chen [a], Wenbin Chen [a], Faqing Ye [b, **], Xiaohui Zheng [a, ***], Zhiguo Liu [a, *]

[a] Chemical Biology Research Center at School of Pharmaceutical Sciences, Wenzhou Medical University, 1210 University Town, Wenzhou, Zhejiang, 325035, China
[b] School of Pharmaceutical Sciences, Wenzhou Medical University, 1210 University Town, Wenzhou, Zhejiang, 325035, China

ARTICLE INFO

Article history:
Received 4 October 2020
Received in revised form
25 December 2020
Accepted 11 January 2021
Available online 24 January 2021

Keywords:
N-substituted benzamides
Osteosarcoma
Anti-migration
Activity

ABSTRACT

A novel series of novel *N*-substituted (indole or indazole) benzamides were synthesized, and their anti-tumor properties were evaluated. The majority of tested compounds possessed moderate cytotoxicity, but inspiringly, we verified that active compound **5d** presents an astonishing advantage by inhibiting the adhesion, migration, and invasion of osteosarcoma (OS) cells *in vitro*. Mechanistically, we confirmed **5d** inhibited the migration ability of OS cells via the expression of genes related to adhesion, migration, and invasion. This effects of **5d** suggest that it can be used as a potential chemotherapeutic drug to some aggressive and/or metastatic cancers, as well as in combination with other clinical anti-cancer drugs. In turn, this could enhance the therapeutic effect or reduce the risk of cell migration.

1. Introduction

Osteosarcoma (OS) is the most common type of primary bone malignancy, with high recurrence and metastasis. OS patients, especially adolescent osteosarcoma, have a median overall survival time of less than 12 months after diagnosis, and no standard treatment strategy has been established [1–3]. Currently, chemotherapy, adjuvant chemotherapy, and postoperative chemotherapy are still the primary therapeutic strategies for OS treatment, the cisplatin, methotrexate, doxorubicin, and etoposide are the most commonly used antitumor drug in the chemotherapy of OS [4,5]. However, clinical studies suggested that these therapeutic strategies had limited chemotherapy effect towards OS, due to the subsequent drug resistance and the migration of cancer cells. In order to achieve necessary antitumor effects, large doses of drugs are often adopted in practice. For example, high-dose methotrexate, a combination of doxorubicin and cisplatin, has become the standard treatment plan for OS in most medical centers in the United States and Europe [4,6–9]. However, the disadvantages of high-dose chemotherapy regimens cannot be neglected. Large numbers of clinical data indicate that high dose drug maintenance chemotherapy leads to serious side effects, such as thrombocytopenia, liver and kidney toxicity, and other side effects [4,7,10–12]. Faced with the current dilemma, it is extremely urgent to develop new drugs to treat aggressive malignant adolescent osteosarcoma.

IMD-0354 (N-(3,5-bis(trifluoromethyl)phenyl)-5-chloro-2-hydroxybenzamide, Fig. 1) was clinically developed for atopic dermatitis (AD) patients in phase I [13–15]. It can induce apoptosis, inhibit proliferation, and overcome multidrug resistance of various tumor cells [14–18]. *N*-phenylbenzamide, the main scaffold of IMD-0354, is found in many drugs commonly used for the treatment of cancer [19–22]. Moreover, the previous structure-activity analysis suggested that the hydroxyl group and the meta-chloro substituent on ring A appeared to play an important role in the inhibitory activity. The indole heterocyclic system is an important scaffold among the most studied pharmacophore groups in drug research studies [23–25]. Also, some indazole derivatives have been identified as attractive new classes of drug candidates for anticancer therapy [26–30]. As part of our ongoing anti-cancer drug discovery

* Corresponding author.
** Corresponding author.
*** Corresponding author.
E-mail addresses: yfq664340@163.com (F. Ye), zhengxh@wmu.edu.cn (X. Zheng), lzgcnu@163.com (Z. Liu).
[1] These authors contribute equally to this work.

https://doi.org/10.1016/j.ejmech.2021.113203
0223-5234/

Abbreviation

Osteosarcoma (OS)
N-(3,5-bis(trifluoromethyl)phenyl)-5-chloro-2-hydroxybenzamide (IMD-b)
Atopic dermatitis (AD)
Dimethyl Formamide (DMF)
Tetrahydrofuran (THF)
3-(4,5-Dimethylthiazol-2-yl)-2,5-diphenyl tetrazolium bromide (MTT)
Dimethyl sulfoxide (DMSO)
Optical density value (OD value)
Focal adhesion kinase (FAK)
Phospho- Focal adhesion kinase (Tyr397) (p-FAK)
Immunofluorescence (IF)
Ribonucleic Acid (RNA)
RNA Sequencing (RNA-seq)
Adenosine triphosphate (ATP)
Flow cytometry (FCM)
5,5′,6,6′-Tetrachloro-1,1′,3,3′-tetraethyl-imidacarbocyanine iodide (JC-1)
Deoxyribonucleic acid (DNA)
P53-binding protein 1 (53BP1)
DNA double-strand breaks (DSBs)
Replication Protein A (RPA)
Thin layer chromatography (TLC)

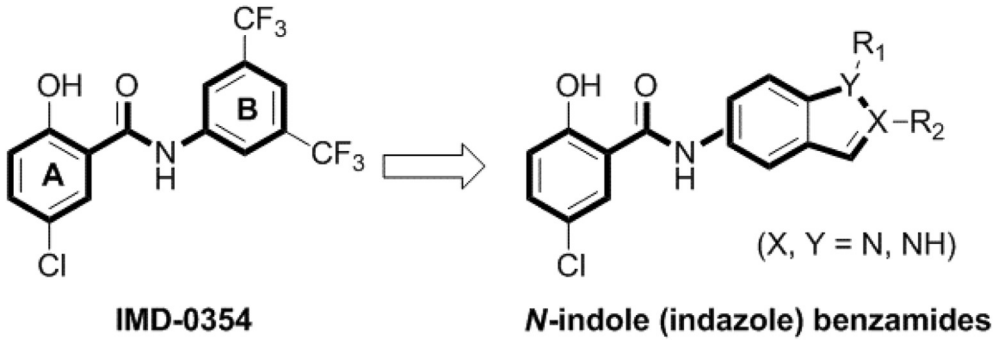

Fig. 1. The chemical structure of IMD-0354 and drug design conception.

activities, we aim to find lead compounds with a new structural skeleton for the treatment of OS. Thus, we envisioned that the replacement of the phenyl moiety of *N*-phenylbenzamide scaffold in IMD-0354, with substituted indole or indazole fragments, would yield a novel series of *N*-substituted (indole or indazole) benzamides with potent anti-cancer activity.

The present study describes the preparation of *N*-substituted (indole or indazole) benzamides whose structures are similar to compounds IMD-0354, as well as their anti-proliferative and anti-migration activities [22,31,32]. Among these newly synthesized compounds, 5d showed the most promising anti-proliferative effects on human osteosarcoma U2OS and MG63 cells. Furthermore, a gene-expression model was also used to detect molecular-level changes related to adhesion, migration, and invasion genes in OS cells, under the influence of active compound 5d, by RNA-Seq technology release.

2. Result and discussion

2.1. Chemistry

The *N*-substituted benzamides **4a**–**4g** and **5a**–**5d** were prepared as shown in Scheme 1. Acetylation of commercially available 5-chloro-2-hydroxybenzoic acid with oxalyl chloride and catalytic amounts of dimethylformamide (DMF) under wild conditions provided 2-acetoxy-5-chlorobenzoic acid (**3**). The intermediate compound **3** reacted with acetyl chloride to obtain corresponding acyl chloride, which underwent condensation with different indolamine or indazolamine, followed by deprotection of the acetyl group to yield desired compounds **4a**–**4g**. Compounds **5a**–**5d** were achieved by benzylation of *N*-1 in various indolamine or indazolamine structures in the presence of benzyl chloride, sodium hydride, and tetrahydrofuran (THF).

The synthetic routes of 5-chloro-2-hydroxy-benzamide derivatives **11a**–**11f** are shown in Scheme 2. THP-protection of indazole, followed by reduction of the nitro group in 4-nitro-1H-indazole (**5**), gave 1-(tetrahydro-2H-pyran-2-yl)-1H-indazol-4-amine (**6**). Conversely, benzylation of the phenol in 5-chloro-2-hydroxybenzoic acid (**2**) with benzyl chloride yielded benzoic acid (**7**), and amide condensation reaction between amine **6** and benzoic acid **7** lead to benzamide **8** through the same process as preparing **4a**–**4g**. Treatment of trifluoroacetic acid afforded THP deprotected benzamide **9**, which then underwent amide condensation with various acyl chlorides to give benzamides **10a**–**10f**. Accordingly, benzyl deprotection of **10a**–**10f** using hydrogen and 10% palladium on carbon (H_2, 10%Pd/C) provided compounds **11a**–**11f**.

Alternatively, treatment of benzamide **9** with various alkyl halides or dimethylcarbamic chloride under basic conditions afforded **12a**–**12d** and its respective analogs **13a**–**13d**. Finally, compounds **14a**–**14d** and their respective analogs **15a**–**15d,** as well compounds **16a** and **17a**, were achieved successfully by benzyl deprotection and ester hydrolysis procedures, as described in Scheme 3. The structures of all new compounds were fully characterized by proton nuclear magnetic resonance (^{1}H NMR), carbon nuclear magnetic resonance (^{13}C NMR), and electrospray ionization mass spectrometry (ESI-MS).

2.2. Anti-proliferative effects of the synthetic compounds

Newly synthesized compounds were assessed for cytotoxicity against two human osteosarcoma cell lines, U2OS (bone

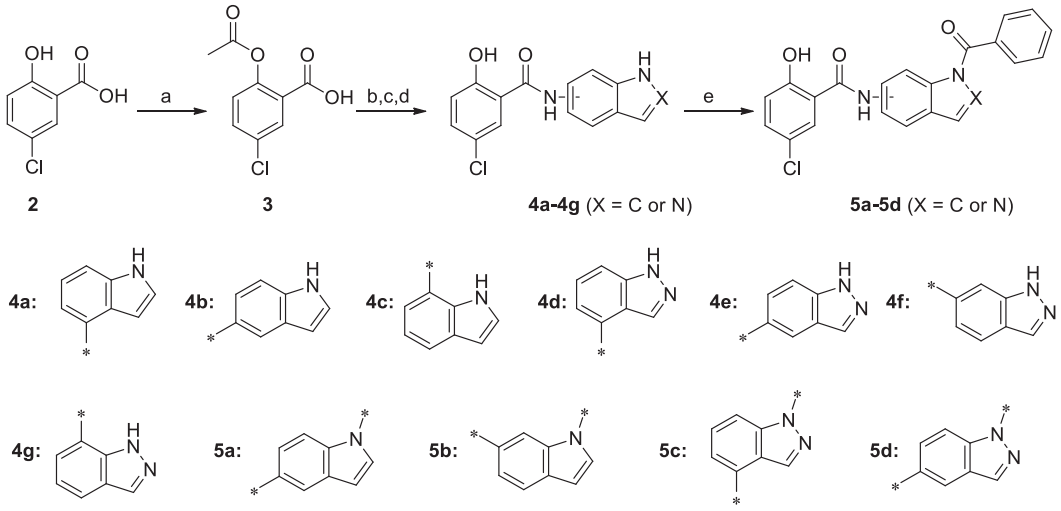

Scheme 1. Synthetic route and structures of *N*-substituted benzamides **4a-4g** and **5a-5d**. Reagents and conditions: a) Oxalyl chloride, DMF,CH_2Cl_2, rt; b) Oxalyl chloride, Et_3N, THF, rt; c) Various Amino indole (indazole), Et_3N, CH_2Cl_2, rt; d) 1 M NaOH, THF/MeOH; e) Benzoyl chloride, NaH, THF, rt.

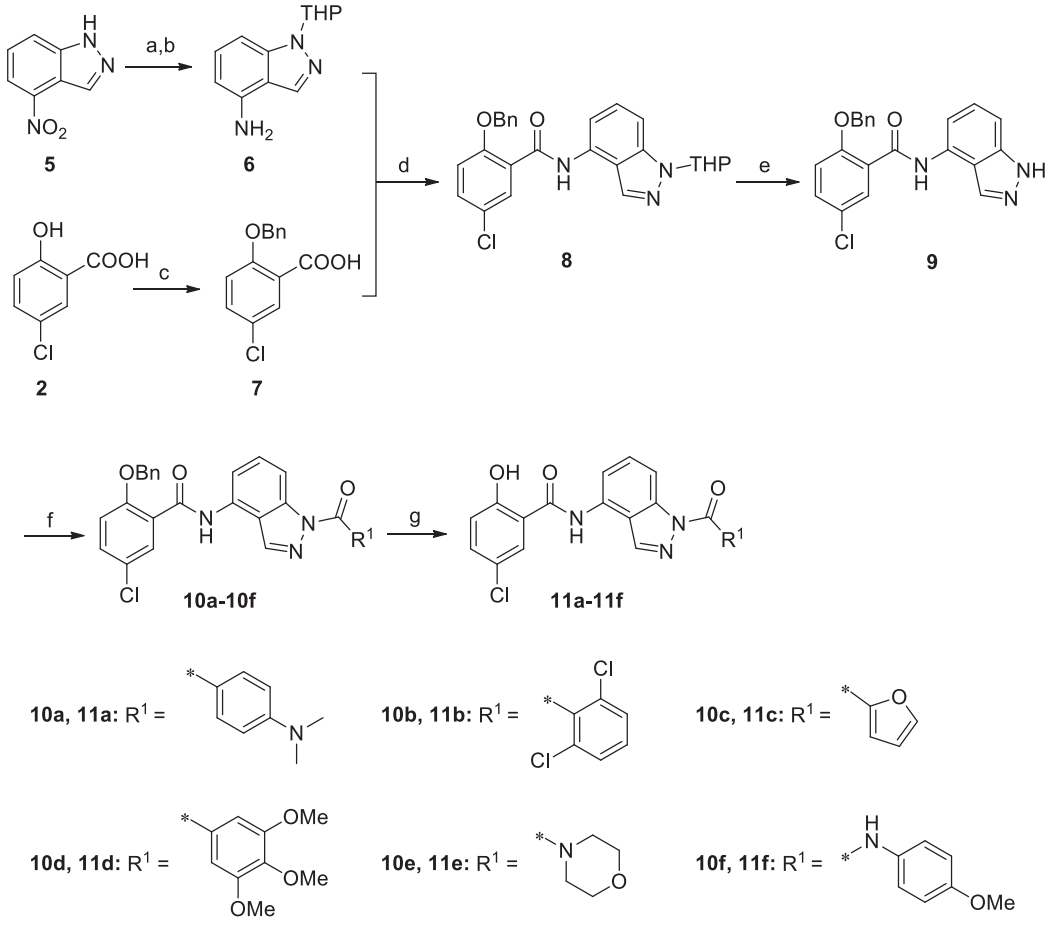

Scheme 2. Synthetic routes and structures of *N*-substituted benzamides **11a-11f**. Reagents and conditions: a) 3,4-dihydro-2H-pyran, PPTS, CH_2Cl_2, rt; b) Pd/C (20%), H_2, THF, rt; c) BnCl, K_2CO_3, DMF, rt; d) Oxalyl chloride, CH_2Cl_2, catalyzed DMF, Et_3N, 0 °C-rt; e) CF_3COOH, CH_2Cl_2, rt; f) NaH, various acyl chlorides, THF, rt; g) 10%Pd/C, H_2, rt.

osteosarcoma epithelial cells) and MG63 (osteoblast-like cells). The cell viability was evaluated at a single concentration of 40 μM for 48 h by MTT assay, and IMD-0354-treated cells were used as a positive control. Although the majority of compounds did not exhibit any significant inhibited potency, compounds **5c**–**5d** with (1H-indazol-1-yl)(phenyl)methanone, **11d** with (1H-indazol-1-yl)(3,4,5-trimethoxyphenyl)methanone, **14c** with 2-(1H-indazol-1-yl)-*N*,*N*-dimethylacetamide, and **15d** with N,N-dimethyl-2H-

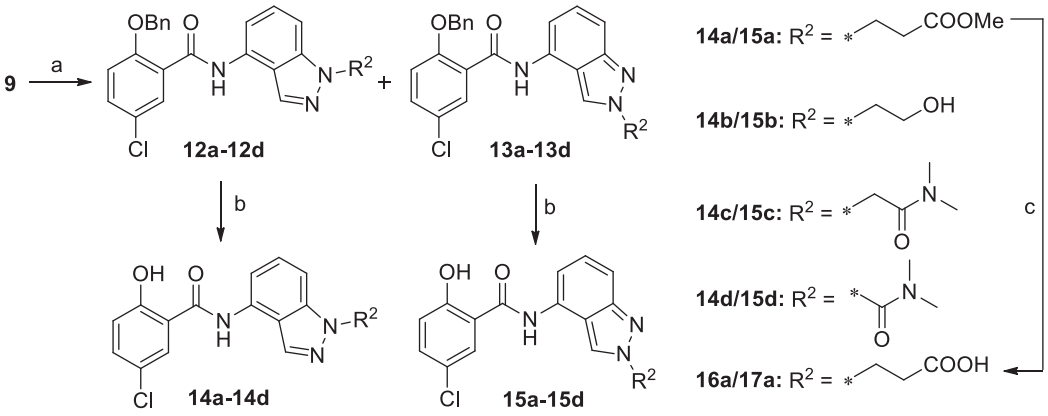

Scheme 3. Synthetic routes and structures of *N*-substituted benzamides **12a-12d**, **13a-13d**, **14a-14d**, **15a-15d**, **16a**, and **17a**. Reagents and conditions: a) NaH, various alkyl halides or dimethylcarbamic chloride, THF, rt; b) 10%Pd/C, H_2, rt; c) NaOH (10%), MeOH, rt, 3 h, then 6 *N*-HCl.

indazole-2-carboxamide moieties showed different levels of inhibition for cell proliferation against both cell lines (Fig. 2A and B). Importantly, **5d** (N-(1-benzoyl-1H-indazol-5-yl)-5-chloro-2-hydroxybenzamide) displayed the greatest inhibitory effect against cancer cell lines U2OS and MG63, and the cell viabilities (%) were 39.5% and 36.0%, respectively. Based on the preliminary cytotoxicity, it is difficult to analyze the structure-activity relationships (SARs) due to their relatively low activity. In general, the derivatives containing the 1H-indazole moiety showed higher cytotoxic activity than that of the indole series, and incorporating larger aromatic substituents on the N-1 position of the indazole seemed to be a more effective, such as compounds **5c**, **5d**, **11d**, and **14c**.

The cytotoxicity and safety of these synthetic compounds were evaluated on human normal liver MIHA cells by MTT assays at a concentration of 40 μM. As shown in Fig. 2C and Table 1, almost all of the compounds exhibited no significant effects for inhibiting cell proliferation, supporting their reasonable safety. At the same time, we compared the NF-κB activity with IMD-0354, the result shown that 5d has more excellent inhibitory ability in Fig. 2D and E.

2.3. Active compound 5d reduces the pseudopodia area of OS cells by suppressing the expression and distribution of focal adhesion kinase (FAK)

Compared to the untreated group, we observed obvious changes in cell morphology, cell antennae, shortening, and the edge of the cell membrane got smoothly, of **5d**-treated (5.0, 10.0, and 20.0 μM) U2OS and MG63 cells in a dose-dependent manner (Fig. 3A). We speculated that **5d** might affect the expression and function of cytoskeletal proteins of OS cells. F-actin is the most abundant protein, and it is a crucial protein for cell stability, morphogenesis, and motility [33–35]. In addition, focal adhesion kinase (FAK) is a cytoplasmic kinase, which is essential for cell migration and morphogenesis [36–38]. To explore whether **5d** treatment affected the expression or activation of FAK and F-actin, immunofluorescence (IF) assays were performed using FAK antibody and phalloidin, a fluorescent dye of F-actin filaggrin. These results show that compared to untreated cells, F-actin and FAK of **5d**-treated OS cells U2OS and MG63 shrank and gathered around nucleus as indicated by the arrows (Fig. 3B and Figure S1A). Moreover, the cell spreading area decreased for 5d-treated cells (Fig. 3C and Figure S1B). In addition, western blot further showed that **5d** efficiently decreased the expression of p-FAK (Fig. 3D and E and Figure S1C, S1E). Taken together, the data verified that active compound **5d** affects the cell morphology by suppressing FAK phosphorylation and FAK/F-actin-cytoskeleton organization.

2.4. Active compound 5d inhibits the adhesion, migration, and invasion of OS cells

Focal adhesion kinase (FAK) is a cytoplasmic tyrosine kinase that plays a key part in cancer cell migration, invasion, and proliferation, the increased expression of phosphorylated FAK in tumor cells is correlated with poor prognosis [36,38,39]. In order to confirm the effect of compound **5d** on cell adhesion, a cell adhesion assay was performed in **5d**-treated and -untreated OS cells U2OS and MG63. The results show that the two cell lines displayed significant decreases in cell adhesion to the matrix after **5d** treatment (5.0, 10.0, and 20.0 μM) in a dose-dependent manner, suggesting that **5d** treatment decreases cell adhesion ability (Fig. 4A and B).

Cell adhesion is often associated with cell migration [40,41]. Therefore, we performed scratch-wound healing assay to determine the migration rate of U2OS and MG63 cells in the presence or absence of **5d**. Our results show that compound **5d** weakens the migration ability of OS cells (Fig. 3C and Figure S2A). After **5d** treatment for 72 h, 70% of the scratch was covered by migrated U2OS cells, while only 23.3% of the scratch was covered in 20.0 μM **5d**-treated cells (Fig. 4D). Similarly, 20.0 μM **5d**-treated MG63 cells showed a significantly decreased migration rate (Figure S2B). These results demonstrate that **5d** inhibited the migration of OS cells.

To further confirm the inhibited migration ability of cancer cells induced by **5d**, the transwell migration assay was performed. The quantitative data demonstrate that the invasion ability of the **5d**-treated OS cells was significantly inhibited, compared to untreated cells (Fig. 4E and Figure S2C). The results indicate that compound **5d** could significantly inhibit OS cells' adhesion, migration, and invasion. Moreover, the results suggest that **5d** can be used as a potential anti-migration drug in some aggressive and/or metastatic cancers, as well as in combination with other clinical anti-cancer drugs to enhance the therapeutic effect or reduce the risk of cancer cell distance migration.

2.5. Compound 5d affects the gene expression of adhesion-, migration-, and invasion-related genes of OS cells

In order to explore the anti-migration mechanisms of **5d** towards OS cells, U2OS, and MG63 at the gene level, transcriptome sequencing (mRNA, Hiseq2000-PE125) was carried out to detect the effect of **5d** on global gene expression in OS cells. The OS cells

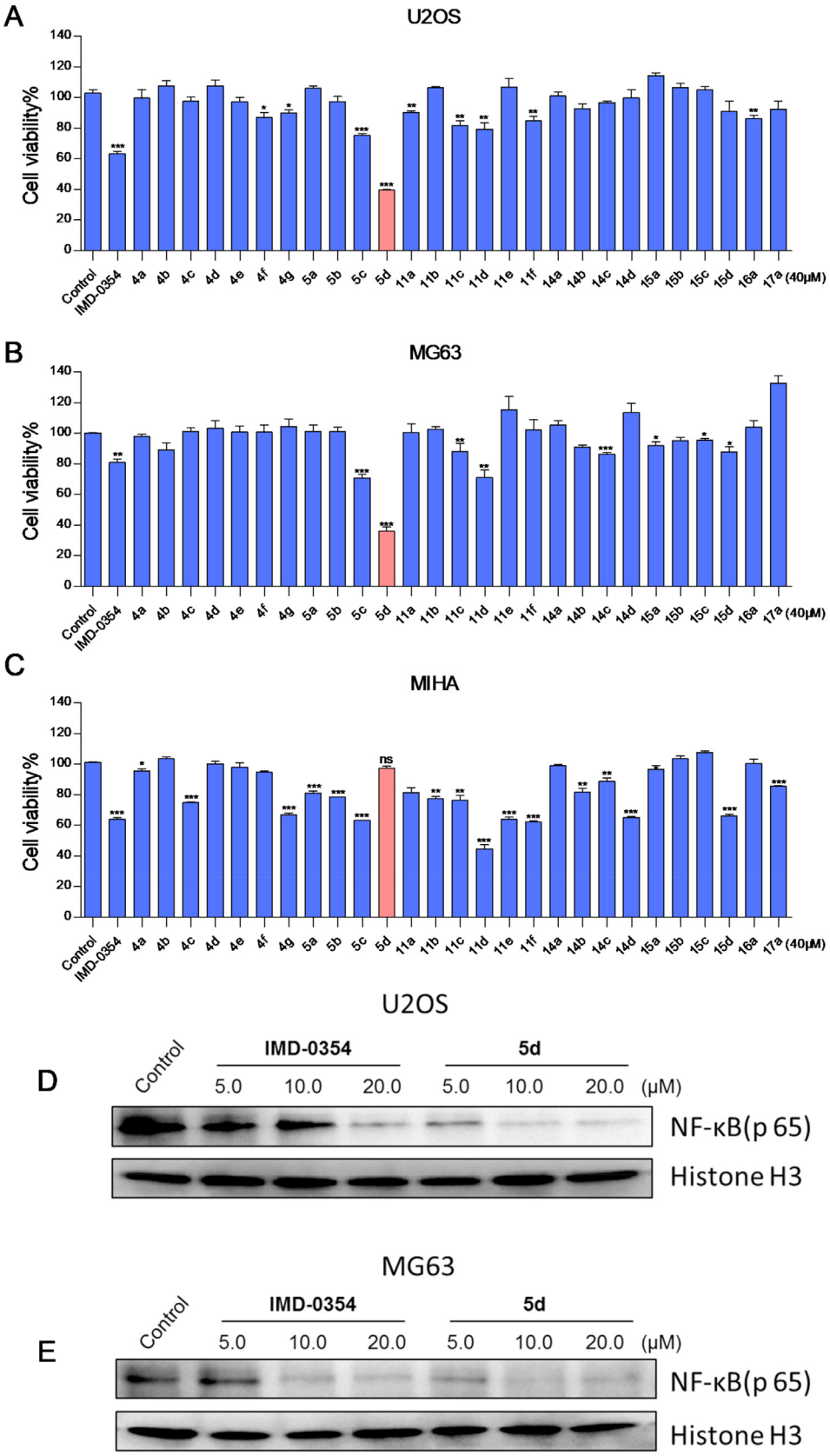

Fig. 2. Synthetic compounds possessed moderate cytotoxicity to OS cells and low toxicity to normal cells. (A–C) U2OS, MG63, and MIHA were pretreated with compounds (40 μM) for 48 h. Cell viability was measured by MTT assay and presented as a percentage of that in the control (0.01% DMSO). (D-E) U2OS and MG63 cells were lysed for Western blot experiment after 48 h of treatment with 0.01% DMSO as the control, 5, 10, and 20 μM concentrations 5d and IMD-0354 respectively for 48 h. Values are the average ± SD of three independent experiments. *$p < 0.05$; **$p < 0.01$; ***$p < 0.001$, vs. control group.

Table 1
IC_{50} (μM) values determined by the MTT assay.

Compd.	IC_{50} (μM)		
	U2OS	MG63	MIHA
5a	>100	35 ± 0.1834	>100
5b	63.02 ± 2.360	74.85 ± 0.470	>100
5c	>100	43.344 ± 4.743	>100
5d	18.67 ± 0.732	20.13 ± 0.798	>100
11c	>100	>100	>100
11d	>100	>100	63.158 ± 2.569
15d	>100	43.344 ± 4.743	>100
IMD-0354	50.91 ± 0.844	48.72 ± 0.8979	>100

were cultured in the presence or absence of 10.0 μM **5d** for 48 h. The mRNA of the cells was isolated and subjected to RNA-seq. The top 100 changes in mRNA transcripts and their abundances are listed in Tables S1 and S2. Full sequence data from these experiments were uploaded to the GEO database under accession number of GSE156729. Changed genes were functionally grouped by GO-biology analysis. Our results show that in U2OS cells, the expression of 1.15% genes changed upon treatment with **5d,** and 16.8% of those genes were functionally related to cell adhesion and migration (Fig. 5A and B, Table S3). To further verify the data, the same RNA-seq assay was performed in **5d**-treated MG63 cells. Consistent with the results from U2OS cells, **5d**-treated MG63 cells displayed the increase of cell adhesion- and migration-related genes (16.7%) (Figure S3A and B, Table S4A and B).

2.6. Active compound 5d effectively inhibits the proliferation of OS cells by inducing cell cycle arrests

Recently, FAK was found to be involved in the cell proliferation process [42–44]. In order to explore whether compound **5d** would affect the proliferation of OS cells, a long-term proliferation assay and colony cloning assay were carried out. As expected, significant proliferation inhibition occurred in **5d**-treated OS cell at concentrations of 5.0, 10.0, and 20.0 μM (Fig. 6A and B). This observation was further supported by the results of the colony cloning assay, suggesting that **5d** treatment resulted in decreased cell-colony formation in a dose-dependent manner (Fig. 6C and Figure S3A).

Additionally, flow cytometry was performed to investigate whether the activity of compound **5d** slowed down the proliferation rate of OS cells by cell cycle arrest. We observed that **5d** arrested U2OS cell at the S phase in a dose-dependent manner. It is worth noting that **5d** treatment increased the percentage of S phase cells and reduced the percentage of cells in the G0/G1 phase, relative to the control. In addition, the percentage of cells in the G2/M phase was slightly elevated (Fig. 6D and E). The results were consistent with the FAK expression inhibition, which confirmed that the expression or activity blockade of FAK significantly inhibits cell proliferation mainly via inducing the blockade of the cell cycle.

The results of the above assays show that active compound **5d** can not only significantly inhibit the adhesion and migration ability of U2OS and MG63 cells in a short period (48 h) but also inhibit the proliferation ability of U2OS and MG63 cells over extended periods of time (Figure S4A-C).

2.7. Compound 5d causes a decrease in mitochondrial membrane potential of OS cells and induce cell apoptosis

It had been reported that FAK is involved in the regulation pathway of mitochondrial membrane potential. Moreover, mitochondria are the primary location of cell ATP production and play an important role in regulating tumor progression to malignancy

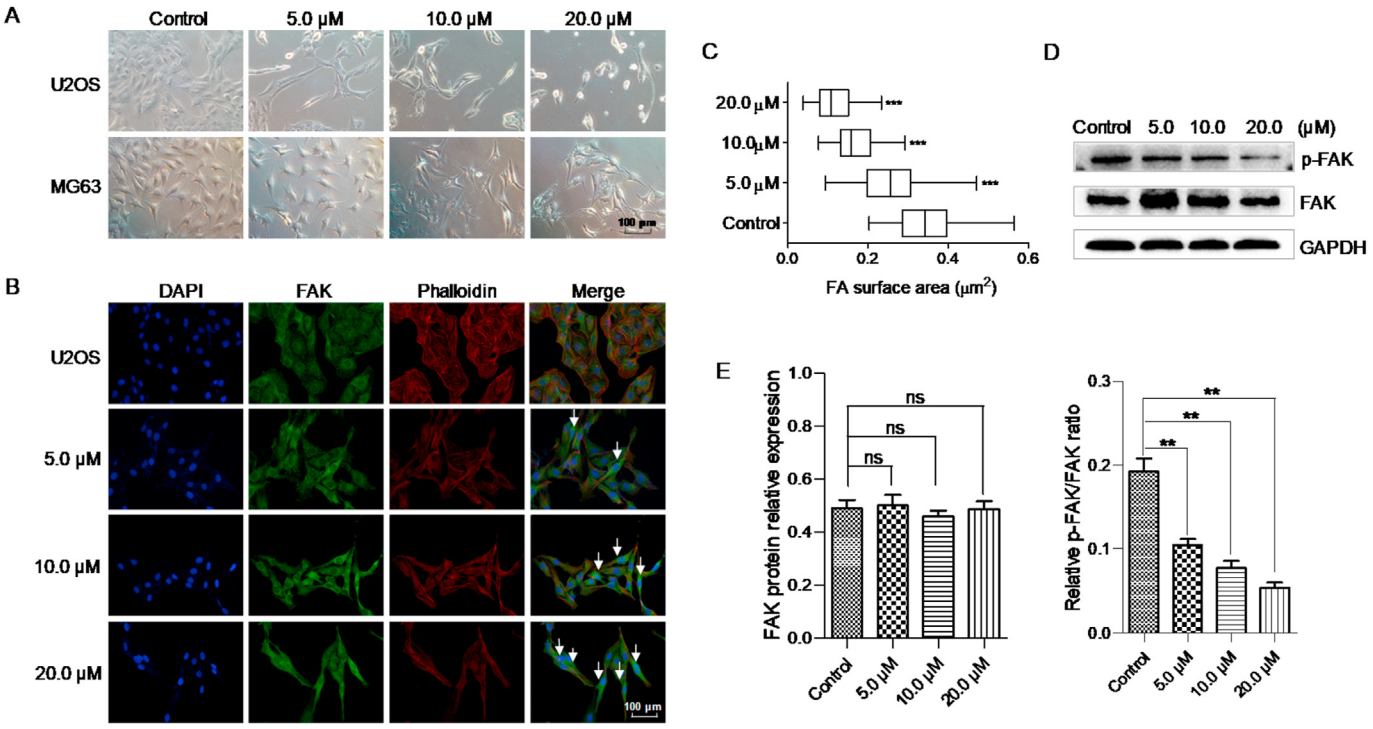

Fig. 3. Active compound **5d** potently suppressed OS cell U2OS and MG63 movement by effecting F-actin expression and FAK activation. (A) U2OS and MG63 cells were treated with **5d** at 5, 10, and 20 μM concentrations for 48 h. (B) U2OS were analyzed by immunofluorescence (IF) assay after treatment with 0 (Control), 5.0, 10.0, and 20.0 μM compound **5d** for 48 h. DAPI (blue), FAK antibody (green), and Phalloidin (red) were detected. (C) Quantification of B. The spreading areas of at least 200 cells were identified and counted using Image J. (D) U2OS cells were lysed for Western blot analysis after 48 h of treatment with 0.01% DMSO (Control) 5.0, 10.0, and 20.0 μM **5d** for 48 h. The expressions of FAK, p-FAK, and GAPDH antibodies were detected. (E)Grey value quantification of data in D. Each result is derived from three independent experiments. Values are the average ± SD of three independent experiments. *$p < 0.05$; **$p < 0.01$; ***$p < 0.001$, vs. Control group.

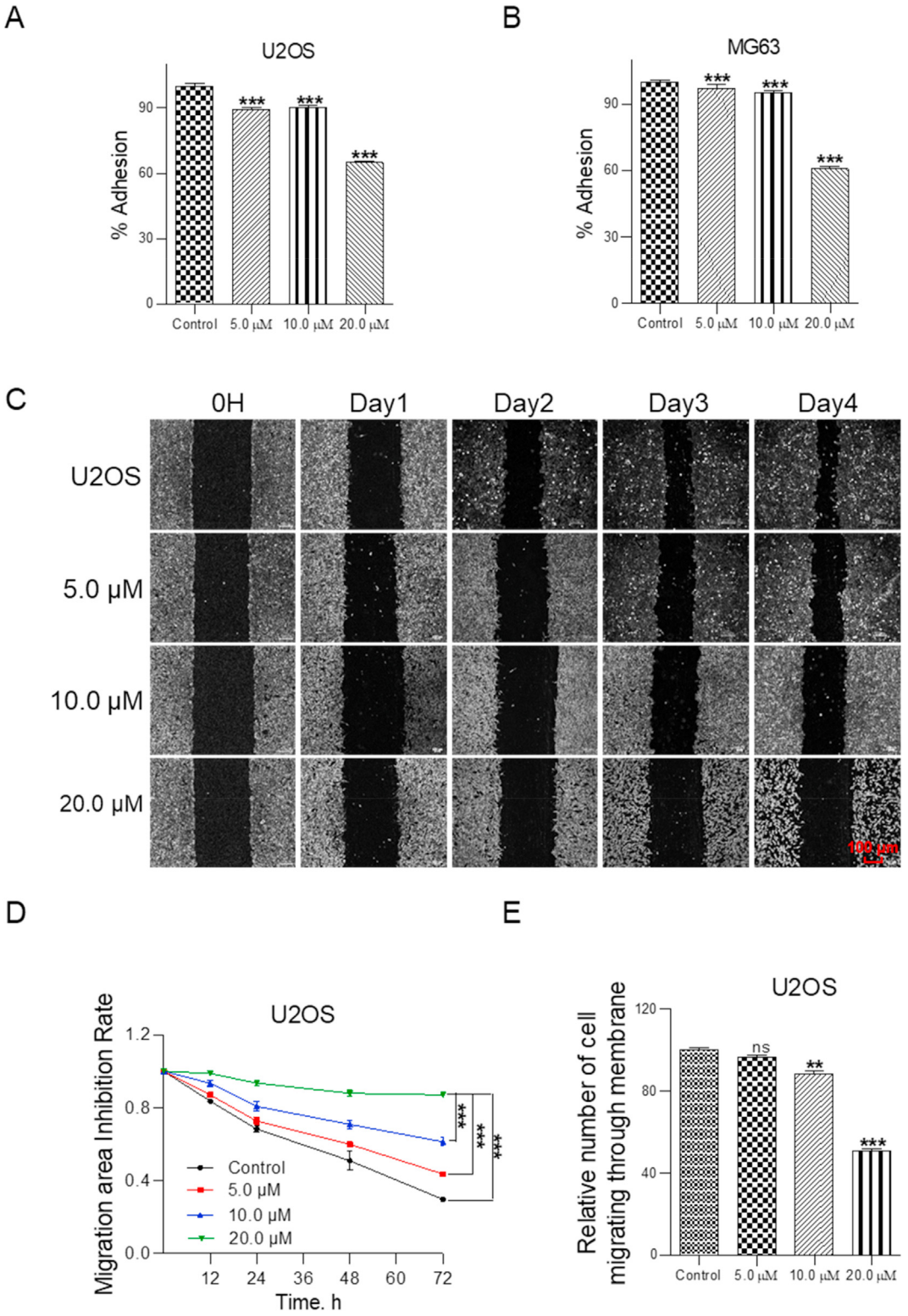

Fig. 4. Compound **5d** inhibits the adhesion, invasion, and migration of OS cells. (A) The adhesion assay was performed to detect the adhesion ability in U2OS cells treated with compound **5d** at 0, 5.0, 10.0, and 20.0 μM concentrations for 48 h. Cells treated with 0.01% DMSO were used as a control (control). (B) Adhesion assay of MG63 cells, cells were pretreated with the indicated concentration of **5d** for 48 h; 0.01% DMSO was used as a control (control). (C) Scratch-wound healing assay to determine the migration rate of U2OS cell in the presence or absence of **5d** for 72 h. (D) Quantification of data in C. (E) Transwell migration assay was performed to detect the migration ability in the absence or presence of the indicated concentration of **5d**. Values are the average ± SD of three independent experiments. *$p < 0.05$; **$p < 0.01$; ***$p < 0.001$, vs. Control.

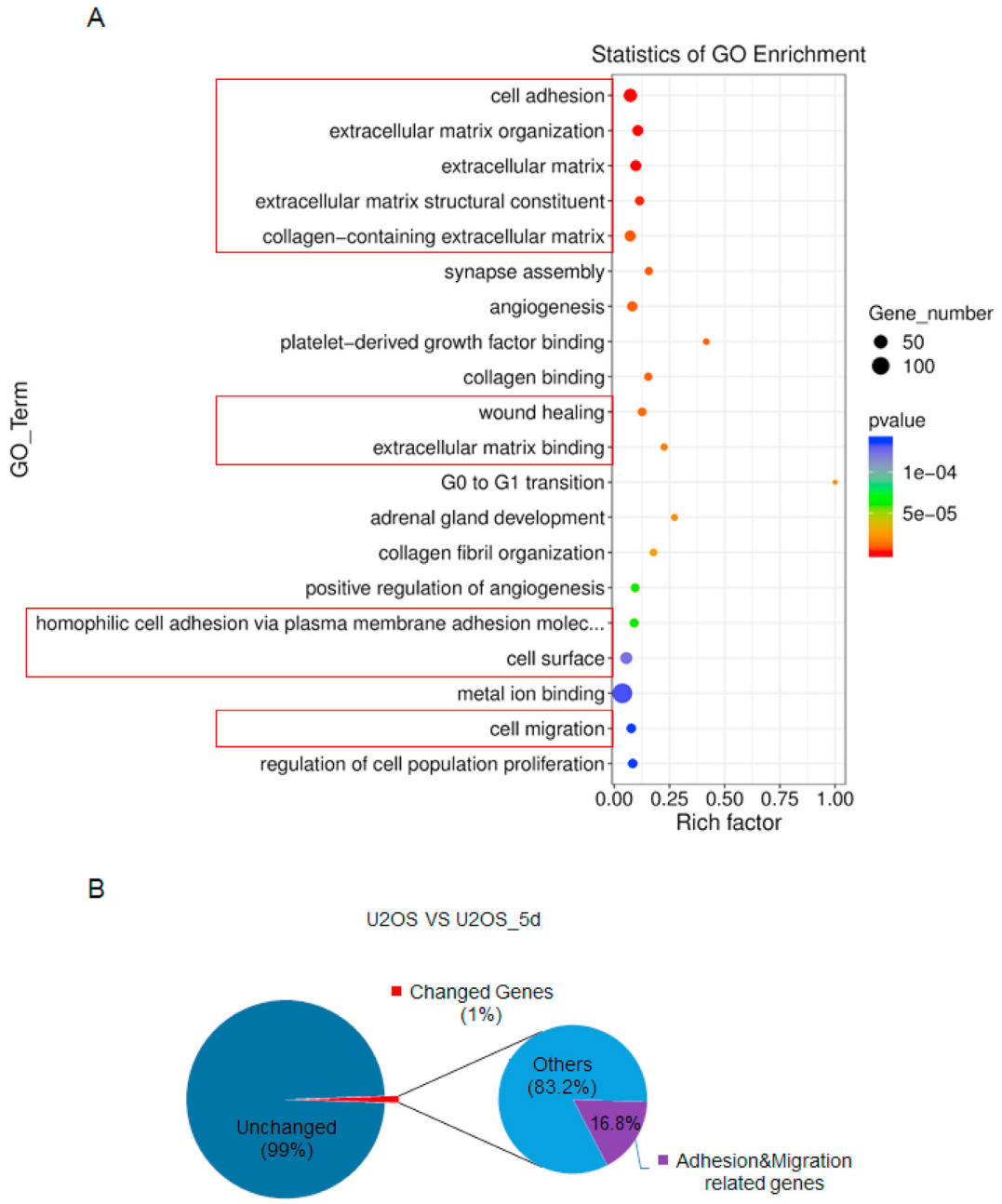

Fig. 5. The expression of genes related to adhesion, migration, and invasion of OS cells was affected by compound **5d**. (A) Analysis of GO enrichment of differentially expressed genes in U2OS cells treated with 10.0 μM **5d** for 48 h. The horizontal axis represents the degree of enrichment (rich factor), and the vertical axis represents the enriched GO term; the size of the dot represents the enrichment in a GO term. The number of differential genes; the color of the dots indicates different p values; the rich factor represents the number of differential genes belonging to a GO term/the total number of genes belonging to this GO. The larger the rich factor, the higher the enrichment of GO term. (B) Statistics of RNA-seq data comparing gene expression in 10.0 μM **5d**-treated for 48 h and -untreated U2OS cells. "GO" analysis showed the functional group of genes changed in expression.

[45]. The formation of pseudopodia, microtubules, and microfilaments requires a large amount of ATP [46–48]. To further explore the role and function of **5d** in OS cells, alterations in mitochondrial membrane potential of U2OS and MG63 cells were analyzed by IF assay with mitochondrial membrane potential fluorescence probe JC-1 staining. In this experiment, OS cells U2OS and MG63 were treated with compound **5d** at concentrations of 5.0, 10.0, and 20.0 μM for 48 h, and then the treated/untreated cells were incubated with the JC-1 fluorescent probe to detect mitochondrial membrane potential. The results of the JC-1 staining assay clearly show that the membrane potentials of U2OS and MG63 cells treated with compound **5d** at 20.0 μM were significantly reduced (Fig. 7A–C and Figure S4A–C). This proves that compound **5d** can indeed reduce the activity of cell mitochondria, affect the energy supply of cells, and affect the motility of cell pseudopodia, which leads to a decrease in the migration and invasion ability of osteosarcoma cells.

Numerous studies have indicated that the down-regulation of FAK activity and cell cycle arrest can cause cell apoptosis. As stated above, **5d** treatment significantly inhibited the expression of FAK in OS cells and the arrest of OS cells in the S phase. In order to explore whether the down-regulation of FAK activity and cell cycle arrest caused by compound **5d** would cause cell apoptosis, a flow cytometric apoptosis assay was conducted. The results show that the

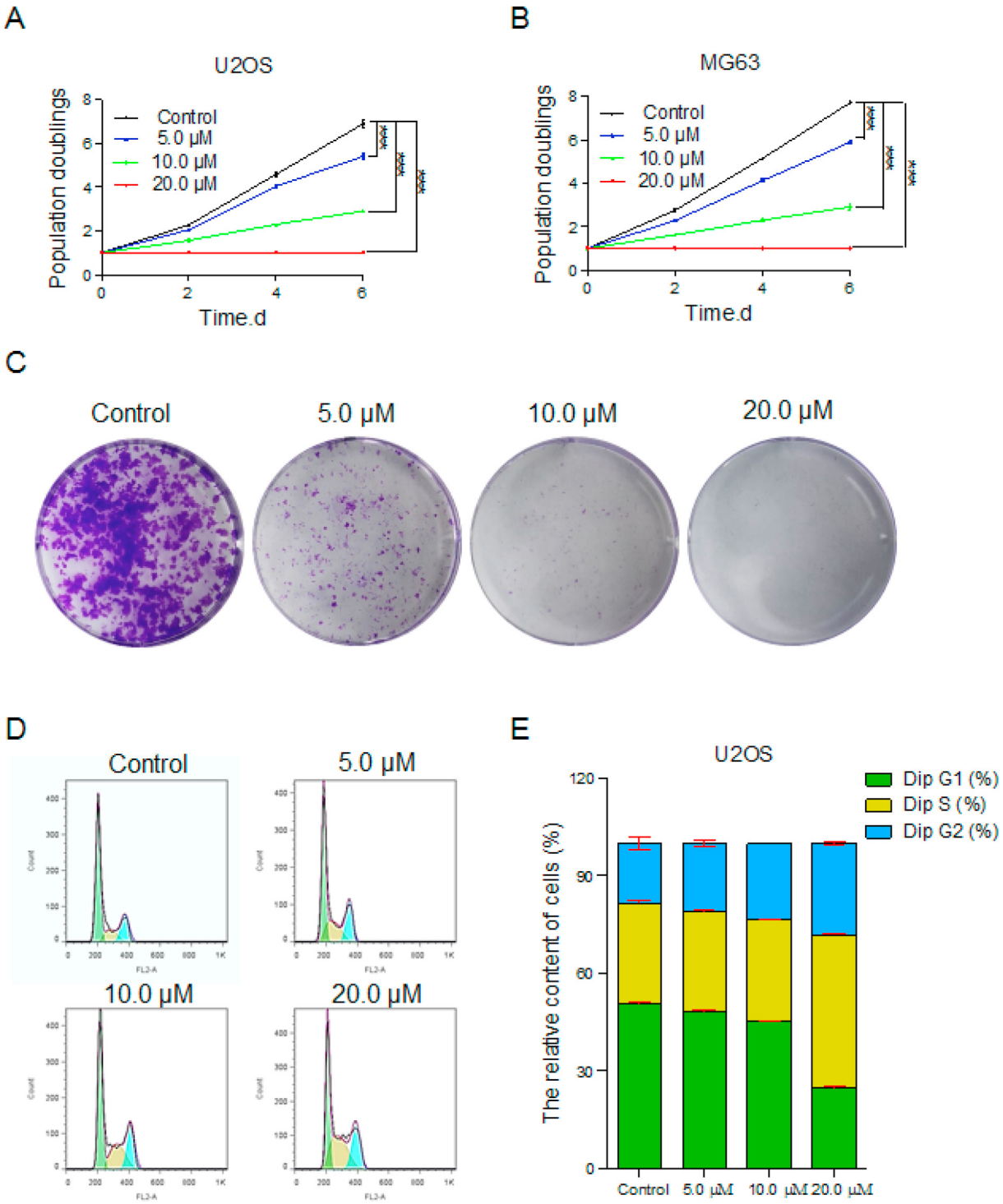

Fig. 6. Active compound **5d** inhibits the proliferation of OS cells by arresting cell cycle of U2OS cell. (A) Proliferation curve of U2OS cells in the presence of **5d** (5.0, 10.0, and 20.0 μM); 0.01% DMSO-treated cells were used as a control. (B) Proliferation curve of MG63 cells with the indicated concentration of **5d** for 48 h; 0.01% DMSO-treated cells were used as a control. (C) Clone formation assay of U2OS cells with the indicated concentration of **5d** for 10 days. (D) FACS analysis of the cell cycle of U2OS cell in the presence or absence of **5d** for 48 h. (E) Quantification of data in (D). Values are the average ± SD of three independent experiments. *$p < 0.05$; **$p < 0.01$; ***$p < 0.001$, vs. Control. Abbreviations: FACS, flow cytometry.

down-regulation of FAK activity caused by 5d cause cell apoptosis after treated with 5d after 72 h (Fig. 8A–C). At the same time, we used western blot to detect the expression of apoptotic related proteins, the results showed that after 72 h of treatment for 5d, Bcl2 protein was significantly reduced, and levels of cleaved-caspase 3 and cleaved-PARP protein were increased (Fig. 8D and E). This is consistent with the results of our streaming experiment. The capacity of 5d causes a decrease in mitochondrial membrane potential to induce apoptosis in human osteosarcoma cells U2OS and MG63. In general, 5d causes a decrease in the mitochondrial

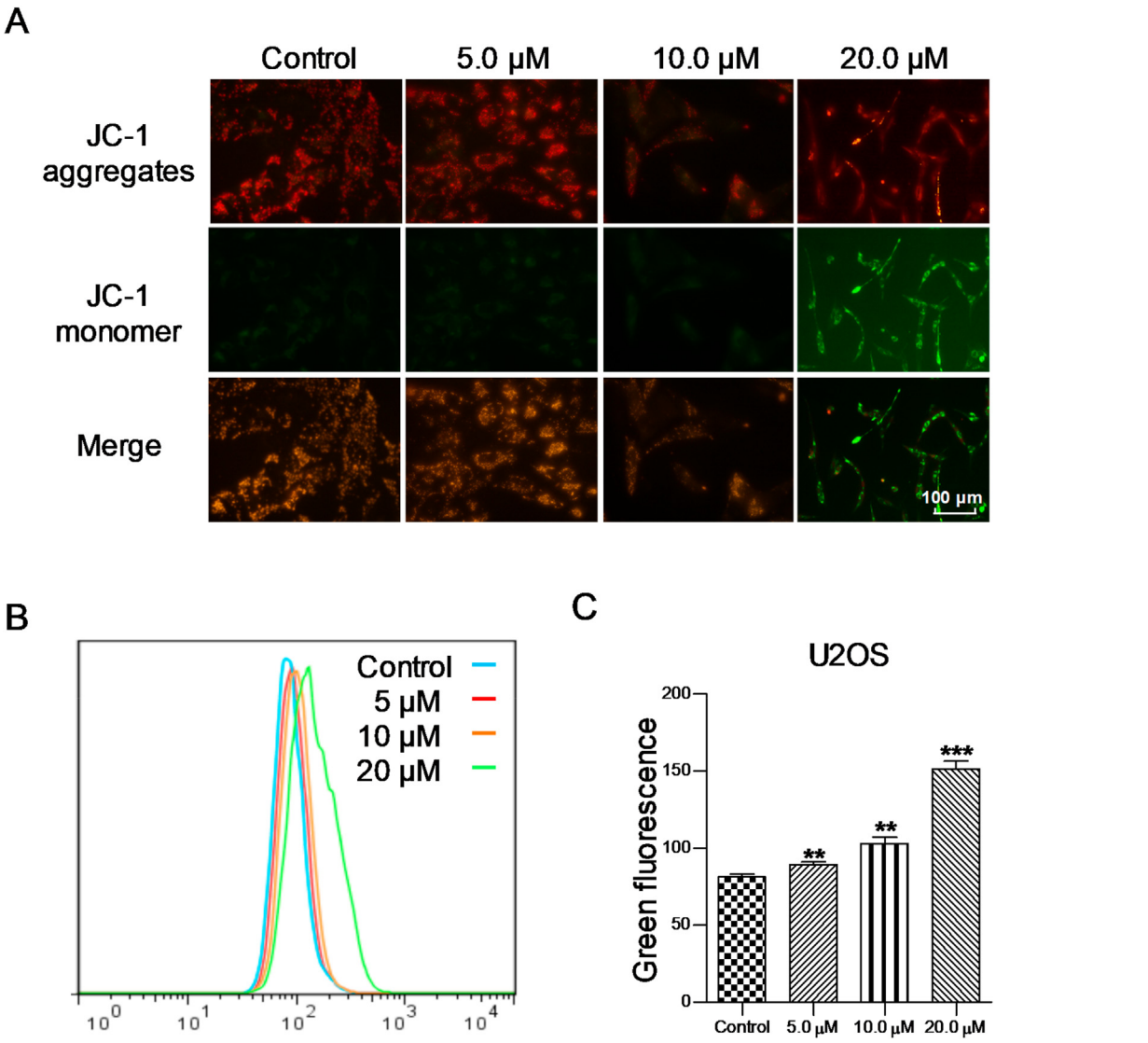

Fig. 7. Compound **5d** causes a decrease in mitochondrial membrane potential of OS cells. (A) JC-1 was used to detect mitochondrial membrane potential of U2OS cells after treatment with 0.01% DMSO (Control), 5.0, 10.0, or 20.0 μM of **5d** for 48 h. J-aggregates (red) and JC-1 monomer (green) were detected. (B) FACS analysis assayed by JC-1 staining on U2OS cells after treatment with **5d**. (C) Quantification of (B). Values are the average ± SD of three independent experiments. *, $p < 0.05$; **, $p < 0.01$; ***, $p < 0.001$, vs. Control. Abbreviations: FACS, flow cytometry.

membrane potential of OS cells in the early stage, and then causes cell apoptosis.

2.8. Active compound 5d treatment triggered intense DNA damage and provoked strong DNA damage response in OS cells

Anticancer drugs, particularly chemotherapy agents, are used to kill cancer cells by introducing mass DNA damage [49]. This is based on the widely accepted concept that non-proliferating cells are more resistant to DNA damage and/or DNA damage response than proliferating cells [50]. Most importantly, as stated above, active compound **5d** induced OS cell arrest in the S phase, which is the critical period of DNA replication throughout the cell cycle. Therefore, we speculate that the underlining anti-migration and anti-proliferation mechanism of **5d** is probably mediated by DNA damage and DNA damage response.

In order to verify this speculation and to further explore the inhibition of compound **5d** on cell migration and proliferation *in vivo*, a series of experiments were carried out sequentially to investigate DNA damage and DNA damage response in 20.0 μM **5d**-treated OS cells for 48 h. The comet assay was performed to assess the level of DNA damage in **5d**-treated or untreated OS cells (Fig. 9A and Figure S7A). As expected, compared to the untreated group, significant DNA damage in **5d**-treated U2OS and MG63 cells was observed, leading to DNA fragments that leave the genome and form "tails" during the comet assay. A percentage of tail DNA was used to indicate the abundance of fragments induced by DNA lesions. In addition, the interference from nuclear condensation and DNA fragmentation caused by apoptosis could be excluded, according to the flow cytometry (FCM) assay. No significant apoptosis was observed after **5d** treatment for 48 h (Figure S6). Accordingly, more than 20% of cells displayed higher DSBs levels than the control (5% tail DNA signal) (Fig. 9B–E and Figure S7B–E).

Significant DNA damage would provoke strong DNA damage repair responses. In order to verify this conjecture, we conducted an IF assay using antibody to 53BP1, which has been widely used as a marker for DSBs (Fig. 9F and Figure S7F) [51,52]. The number of 53BP1 foci per nucleus was calculated in both the control and **5d**-

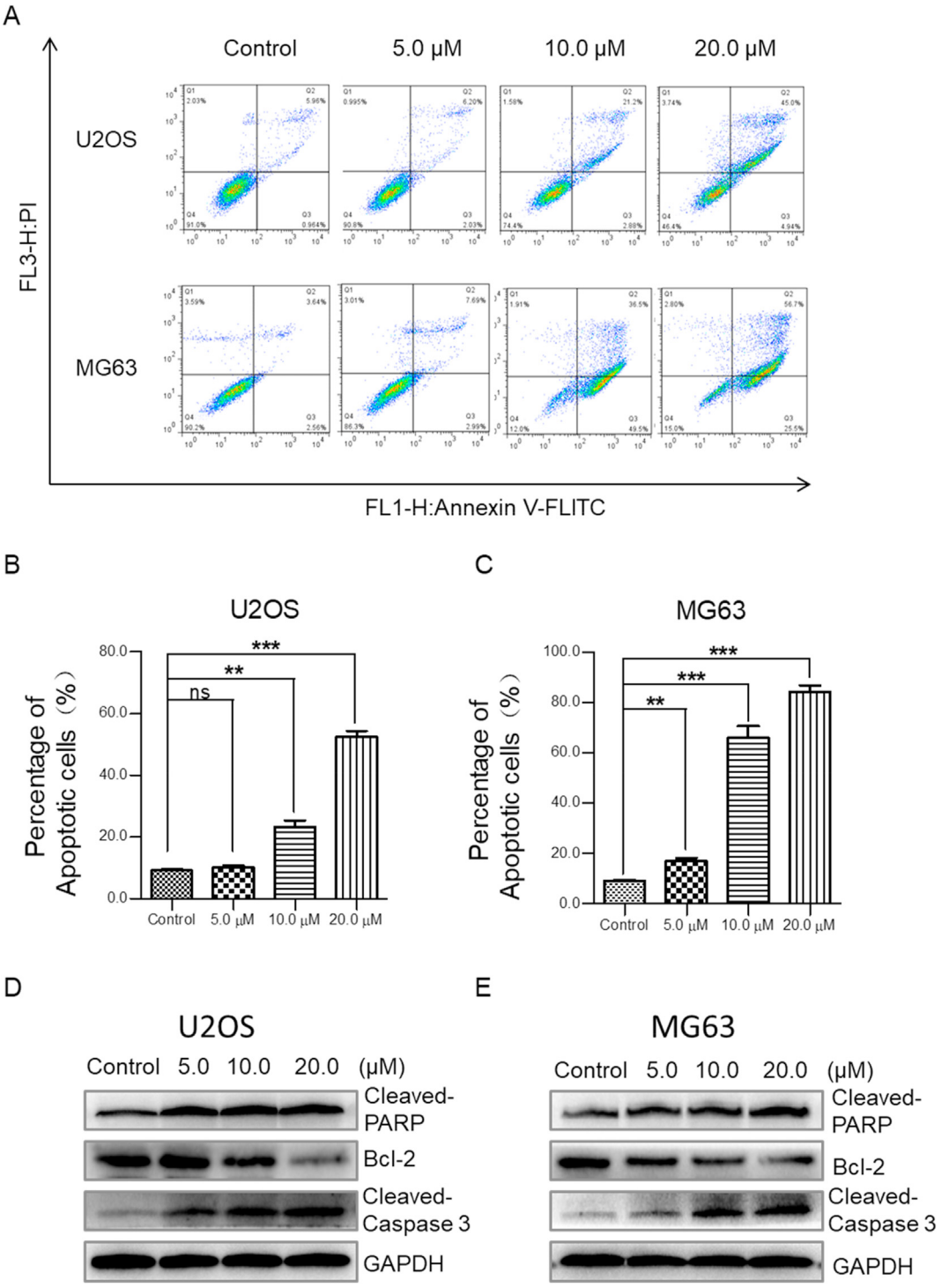

Fig. 8. Compound **5d** induces apoptosis of OS cells after treated for 72 h. (**A**)U2OS and MG63 cells were treated with 0.01% DMSO (Control), 5.0, 10.0 or 20.0 μM of 5d for 72 h, apoptotic cells were assayed by Annexin V/PI staining and FACS analysis. (**B**) (**C**) Quantification of (**A**). (D)U2OS cells were lysed for Western blot experiment after 72 h of treatment with 0.01% DMSO as the control, 5.0, 10.0 or 20.0 μM of 5d for 72 h, (E)MG63 cells were lysed for Western blot experiment after 72 h of treatment with 0.01% DMSO as the control, 5.0, 10.0 or 20.0 μM of 5d for 72 h. Values are the average ± SD of three independent experiments. *, $p < 0.05$; **, $p < 0.01$; ***, $p < 0.001$, vs. Control.
Abbreviations: FACS, flow cytometry; ns, non-significant.

treated U2OS and/or MG63 cells. Unsurprisingly, the number of 53BP1 foci in U2OS cells increased to an average of ~6 foci per nucleus after 20.0 μM treatment for 48 h, and the number of 53BP1 foci per cell in **5d**-treated OS cells was found to be dose-dependent (Fig. 9G and Figure S7G). Furthermore, the levels of DNA damage and DNA damage response of **5d**-treated OS cells were further evaluated by Western blot assay. As shown in Fig. 9H and Supplementary Figure 7H, the molecular markers of DNA double-strand break γH2AX and DNA damage repair protein RPA were both up-regulated, compared with the untreated group [53–55]. The results suggest that compound **5d** triggered significant DNA damage and provoked a strong DNA damage repair response in OS cells.

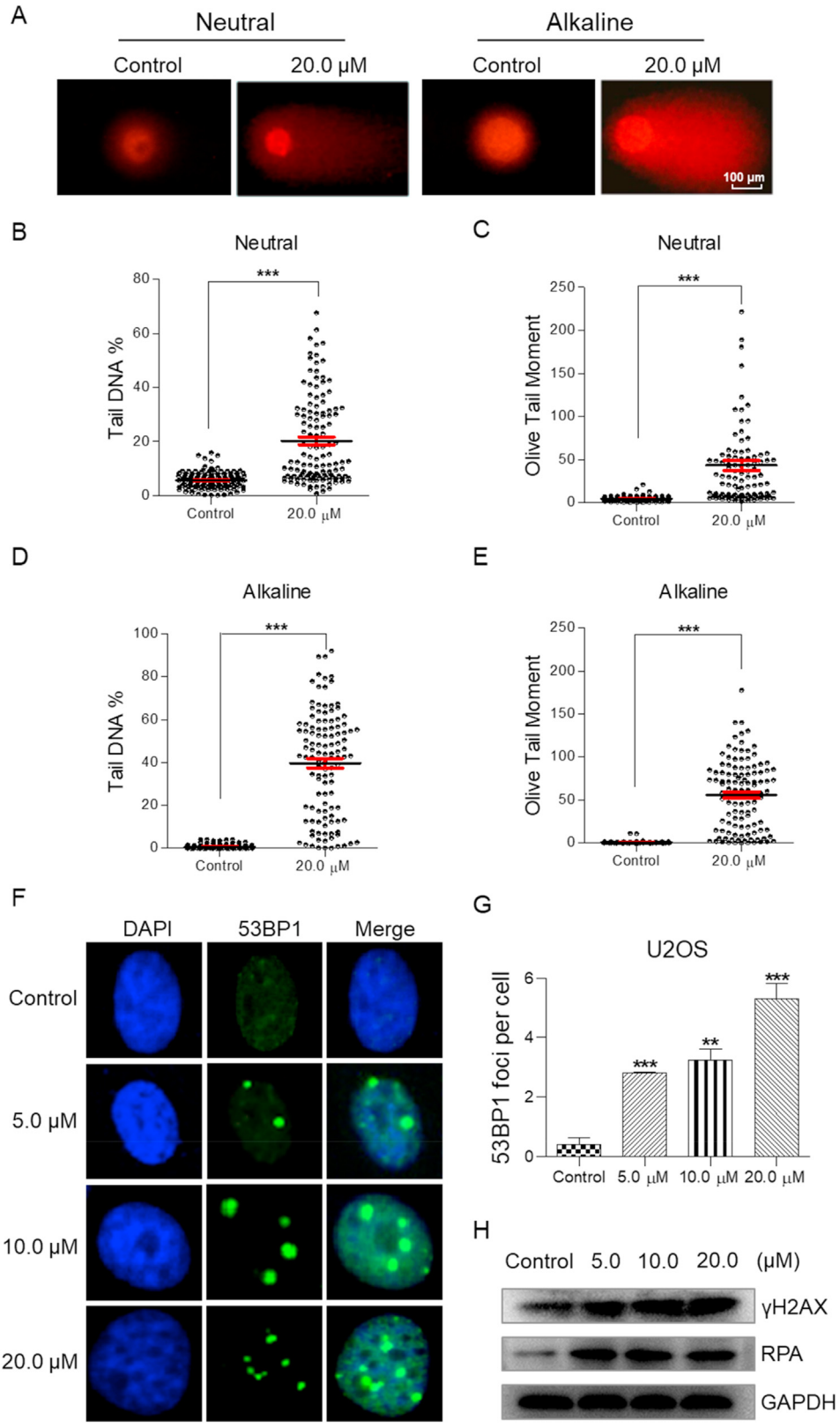

Fig. 9. Active compound **5d** treatment triggered intense DNA damage and provoked strong DNA damage response of OS cells. (A) Comet assay in neutral and alkaline conditions for evaluating the DNA damage of U2OS cell after treatment with 20.0 μM **5d** for 48 h. (B) Quantification of tail DNA (%) under neutral conditions. (C) Quantification of olive tail moment under neutral conditions. (D) Quantification of tail DNA (%) under alkaline conditions. (E) Quantification of olive tail moment under alkaline conditions. (F) IF assay for evaluating the DNA damage response. U2OS cells were treated with 0.01% DMSO (Control), 5.0, 10.0, or 20.0 μM of **5d** for 48 h before the assay. DAPI and 53BP1 were the nucleus dye (blue) and DNA damage marker (green), respectively. (G) Quantification of the numbers of 53BP1 foci. (H) U2OS cells were lysed for Western blot experiment after 48 h of treatment with 0.01% DMSO as the control. Values are the average ± SD of three independent experiments. $*p < 0.05$; $**p < 0.01$; $***p < 0.001$, vs. Control group.

3. Conclusion

We designed and synthesized a series of IMD-0354 derivatives and determined their pharmacological activities in OS cells. During the experiment, we observed significant changes in cell morphology, including contraction of the cell antennae, shortening, and enhanced smoothing of the edge of the cell membrane, in **5d**-treated (5.0, 10.0, and 20.0 μM) U2OS and MG63 cells in a dose-dependent manner. Considering the critical roles of F-actin and FAK in cell stability, morphogenesis and motility, we speculate that **5d** might affect the expression and function of cytoskeletal proteins of OS cells. Considering. In addition, focal adhesion kinase (FAK) is a cytoplasmic kinase, which is essential for cell migration and morphogenesis. The results of the IF assay and western blot analysis verified that active compound **5d** affected the cell morphology by suppressing the FAK phosphorylation and FAK/F-actin-cytoskeleton organization.

The cell adhesion and scratch-wound healing assays were performed in **5d**-treated and -untreated OS cells U2OS and MG63. The results show that the two cell lines displayed significant decreases in cell adhesion and migration ability after **5d** treatment in a dose-dependent manner. Encouraged by these findings, we confirmed the possible mechanisms regarding the anti-migration ability of compound **5d** by RNA-seq assay. Our results show that compound **5d** affects the expression of genes related to adhesion, migration, and invasion of OS cells. All of the above experiments demonstrate that compound **5d** has the ability to inhibit tumor cell migration significantly by impacting gene expression in low concentration. Thus, compound **5d** could become a new, effective anti-migration chemical agent, in combination with antitumor drugs, for different tumor treatment strategies.

Another noteworthy advantage of active compound **5d** is that it inhibits the proliferation ability of OS cells for a long time by inducing cell cycle arrests at a low concentration, with minimal or no toxic side effects on normal cells. This satisfies the need for a long-term medication for clinical treatment of cancer patients.

In summary, although compound **5d** only had moderate anti-tumor proliferation activity, it exhibited a strong anti-migration effect. More importantly, the excellent anti-tumor cell adhesion, invasion, and migration activity of compound **5d** has more gratifying application value in clinic OS therapy. The above advantages show the potential of compound **5d** for clinical application, not only in terms of long-term anti-tumor cell proliferation activity but also in terms of anti-tumor migration. At the same time, the weakening effect of compound **5d** on the anti-tumor migration ability can be used in combination with other clinical drugs that have strong anti-tumor proliferation activity but poor prognosis for aggressive malignant tumors. Furthermore, **5d** provides the possibility of new strategies for clinical treatment methods.

4. Experimental

4.1. General information

All reagents and solvents were purchased from Alfa Aesar and Sigma-Aldrich, respectively. Other chemicals were obtained from local suppliers and were used without further purification. All reactions were performed under nitrogen atmosphere unless otherwise noted. The progress of the reaction was checked via silica gel thin-layer chromatography (250 μ silica gel 60 F_{254} glass plates), and the spots were detected under ultraviolet (UV) light (254 and 366 nm). Column chromatography was performed using Merck silica gel 60 (200–300 mesh ASTM) (Merck KGaA, Darmstadt, Germany). Melting points were determined in a Fisher-Johns melting apparatus and were uncorrected. ^{1}H NMR and ^{3}1C NMR spectra were recorded using a Bruker instrument (Bruker AVANCE DRX-500), and all chemical shifts were given in parts per million relative to tetramethylsilane (TMS). Electron-spray ionization mass spectroscopy (ESI-MS) data were collected in positive mode using a Bruker Esquire 3000t spectrometer.

4.2. Compounds synthesis and characterization

4.2.1. Synthesis of 2-acetoxy-5-chlorobenzoic acid (3)

To a solution of 5-chloro-2-hydroxybenzoic acid (2, 1.71 g, 1.0 mmol) in dry THF (20 mL) was added acetyl chloride (3.7 mL) followed by a catalytic amount of Et_3N (0.01 equiv) and the mixture was stirred overnight at room temperature. The resulting solution was quenched with saturated aqueous NH_4Cl (20 mL). After evaporation of most of the solvent, the mixture was extracted with EtOAc (3 × 20 mL). The aqueous layer was then acidified with 10% HCl to pH 2–3. The precipitated product was filtered and washed with water (50 mL) to yield the desired compound 3 (1.0 g, 46.7%) as a white powder.

4.2.2. General procedures for the synthesis of compounds 4a-4g

To a solution of 3 (110 mg, 0.51 mmol) in dry CH_2Cl_2 (5 mL) at 0 °C was added oxalyl chloride (0.22 mL, 2.55 mmol) dropwise followed by a catalytic amount of DMF (0.05 equiv). The reaction solution was allowed to warm up to room temperature and stirring was continued for 5 h, and then the solvent was removed under reduced pressure, and the residue was dissolved in dry CH_2Cl_2 (5 mL) followed by Et_3N (0.17 mL) and indolamine or indazolamine (0.51 mmol). The mixture was stirred at room temperature and monitored by thin layer chromatography (TLC). The resulting mixture was quenched with saturated NH_4Cl solution (10 mL), and the mixture was extracted with AcOEt (3 × 10 mL). The organic layers were dried over $MgSO_4$ and concentrated at reduced pressure. The residue was dissolved in a solution of THF-MeOH (2:1, 6 mL), 1 moL/L NaOH (1.0 mL) was then added slowly. The reaction solution was stirred for 30 min and diluted with saturated NH_4Cl (10 mL), then extracted with AcOEt (3 × 10 mL). The organic layers were dried over $MgSO_4$ and concentrated at reduced pressure. The residue was purified by chromatography on silica gel providing the target compounds 4a-4g.

4.2.2.1. 1 5-Chloro-2-hydroxy-N-(1H-indol-4-yl) benzamide (4a). Green powder, 23.2% yield, m.p: 226.3–227.5 °C. ^{1}H NMR (500 MHz, DMSO-d_6) δ (ppm): 12.30 (s, 1H), 11.28 (s, 1H), 10.74 (s, 1H), 8.05 (d, J = 2.6 Hz, 1H), 7.77 (d, J = 7.6 Hz, 1H), 7.49 (dd, J = 8.7, 2.7 Hz, 1H), 7.42–7.34 (m, 1H), 7.24 (d, J = 8.1 Hz, 1H), 7.10 (t, J = 8.6 Hz, 2H), 6.45 (s, 1H). ^{13}C NMR (126 MHz, Acetone) δ 167.18, 159.85, 138.16, 134.43, 130.14, 128.82, 125.42, 124.36, 123.16, 122.27, 120.32, 118.63, 114.24, 109.95, 100.08. ESI-MS m/z: 287.2 $(M + H)^+$.

4.2.2.2. 5-Chloro-2-hydroxy-N-(1H-indol-5-yl) benzamide (4b). White powder, 19.41% yield, m.p: 230.4–231.6 °C. ^{1}H NMR (500 MHz, DMSO-d_6) δ (ppm): 7.97 (s, 1H), 7.89 (s, 1H), 7.36–7.29 (m, 3H), 6.88 (d, J = 8.9 Hz, 1H), 6.39 (s, 1H). ^{13}C NMR (126 MHz, Acetone) δ (ppm): 168.19, 161.22, 135.03, 134.49, 130.43, 129.02, 127.59, 126.74, 123.76, 120.52, 117.84, 117.58, 114.76, 112.05, 102.69. ESI-MS m/z: 287.2 $(M + H)^+$.

4.2.2.3. 5-Chloro-2-hydroxy-N-(1H-indol-7-yl) benzamide (4c). White powder, 15.44% yield, m.p: 246.4–247.3 °C. ^{1}H NMR (500 MHz, DMSO-d_6) δ (ppm): 11.34 (s, 1H), 10.92 (s, 1H), 8.03 (s, 1H), 7.47–7.32 (m, 2H), 7.30 (s, 1H), 7.16 (s, 1H), 6.96 (t, J = 7.5 Hz, 1H), 6.91 (d, J = 8.6 Hz, 1H), 6.44 (s, 1H). ^{13}C NMR (126 MHz, DMSO-d_6) δ (ppm): 166.00, 132.88, 129.92, 129.32, 128.28, 125.34, 122.24, 120.04, 118.78, 118.46, 117.61, 116.02, 101.47. ESI-MS m/z:

287.2 $(M + H)^+$.

4.2.2.4. 5-Chloro-2-hydroxy-N-(1H-indazol-4-yl)benzamide (4d). Yellow powder, 33.42% yield, m.p: 307.5–308.4 °C. ^{1}H NMR (500 MHz, DMSO-d_6) δ (ppm): 13.20 (s, 1H), 11.15 (s, 1H), 8.10 (s, 1H), 7.99 (s, 1H), 7.76 (s, 1H), 7.47 (d, J = 7.1 Hz, 1H), 7.34 (d, J = 6.1 Hz, 2H), 7.07 (d, J = 8.3 Hz, 1H). ^{13}C NMR (126 MHz, DMSO-d_6) δ (ppm): 163.98, 157.00, 140.83, 132.95, 131.14, 130.36, 129.05, 126.65, 122.49, 120.00, 119.32, 116.35, 111.24, 106.32. ESI-MS m/z: 288.1 $(M + H)^+$.

4.2.2.5. 5-Chloro-2-hydroxy-N-(1H-indazol-5-yl)benzamide (4e). White powder, 19.12% yield, m.p: 268.1–269.3 °C. ^{1}H NMR (500 MHz, DMSO-d_6) δ (ppm): 13.06 (s, 1H), 12.06 (s, 1H), 10.47 (s, 1H), 8.17 (s, 1H), 8.08 (s, 1H), 8.04 (s, 1H), 7.55 (s, 2H), 7.47 (d, J = 8.6 Hz, 1H), 7.03 (d, J = 8.7 Hz, 1H). ^{13}C NMR (126 MHz, DMSO-d_6) δ (ppm): 165.29, 157.38, 137.41, 133.57, 133.03, 130.67, 128.11, 122.69, 122.60, 121.75, 119.15, 119.00, 112.18, 110.15. ESI-MS m/z: 288.1 $(M + H)^+$.

4.2.2.6. 5-Chloro-2-hydroxy-N-(1H-indazol-6-yl) benzamide (4f). Green powder, 21.42% yield, m.p: 290.3–291.1 °C. ^{1}H NMR (500 MHz, DMSO-d_6) δ (ppm): 13.00 (s, 1H), 11.81 (s, 1H), 10.55 (s, 1H), 8.21 (s, 1H), 8.01 (s, 1H), 7.97 (s, 1H), 7.73 (d, J = 7.5 Hz, 1H), 7.47 (d, J = 8.3 Hz, 1H), 7.24 (d, J = 7.7 Hz, 1H), 7.03 (d, J = 7.6 Hz, 1H). ^{13}C NMR (126 MHz, DMSO-d_6) δ (ppm): 164.95, 156.65, 140.19, 136.15, 133.36, 132.91, 128.45, 122.72, 120.64, 119.94, 119.74, 119.06, 115.25, 100.76. ESI-MS m/z: 288.1 $(M + H)^+$.

4.2.2.7. 5-Chloro-2-hydroxy-N-(1H-indazol-4-yl) benzamide (4g). Red powder, 39.43% yield, m.p: 240.6–242.3 °C. ^{1}H NMR (500 MHz, DMSO-d_6) δ (ppm): 12.94 (s, 1H), 12.08 (s, 1H), 10.63 (s, 1H), 8.13 (s, 2H), 7.68 (d, J = 7.9 Hz, 1H), 7.52 (d, J = 8.4 Hz, 1H), 7.46 (d, J = 7.1 Hz, 1H), 7.14 (t, J = 7.6 Hz, 1H), 7.05 (d, J = 8.7 Hz, 1H). ^{13}C NMR (126 MHz, DMSO-d_6) δ (ppm): 166.21, 158.09, 134.91, 133.74, 133.37, 128.26, 124.49, 122.44, 120.78, 120.70, 120.31, 119.20, 118.30, 118.19. ESI-MS m/z: 288.1 $(M + H)^+$.

4.2.3. General procedures for the synthesis of compounds 5a-5d

To a solution of 1.0 mmol compounds **4a**, 5-chloro-2-hydroxy-*N*-(*1H*-indol-6-yl) benzamide (prepared using the same procedure as for compounds **4a-4g**), 4d and 4e in dry THF (10 mL) was added sodium hydride (35 mg, 1.5 mmol) slowly at room temperature. After 30 min, benzoyl chloride (210 mg, 1.5 mmol) was added. The mixture was stirred at this temperature for 5 h. The reaction mixture was quenched with saturated aqueous NH_4Cl (20 mL), and the mixture was extracted with AcOEt (3 × 20 mL). The organic layers were dried over $MgSO_4$ and concentrated at reduced pressure. The residue was purified by chromatography on silica gel providing the target compounds **5a-5d**, respectively.

4.2.3.1. N-(1-benzoyl-1H-indol-5-yl)-5-chloro-2-hydroxybenzamide (5a). Grey powder, 39.21% yield, m.p: 260.2–262.1 °C. ^{1}H NMR (500 MHz, DMSO-d_6) δ (ppm): 11.98 (s, 1H), 10.55 (s, 1H), 8.27 (d, J = 8.9 Hz, 1H), 8.15 (d, J = 1.7 Hz, 1H), 8.03 (d, J = 2.6 Hz, 1H), 7.82–7.74 (m, 2H), 7.70 (t, J = 7.4 Hz, 1H), 7.61 (t, J = 7.4 Hz, 3H), 7.48 (dd, J = 8.8, 2.6 Hz, 1H), 7.41 (d, J = 3.7 Hz, 1H), 7.03 (d, J = 8.8 Hz, 1H), 6.79 (d, J = 3.7 Hz, 1H). ^{13}C NMR (126 MHz, DMSO-d_6) δ (ppm): 168.01, 165.08, 157.13, 134.03, 133.92, 133.05, 132.30, 132.00, 130.83, 128.94, 128.87, 128.69, 128.28, 122.70, 119.25, 119.13, 118.53, 115.86, 113.16, 108.65. ESI-MS m/z: 391.0 $(M + H)^+$.

4.2.3.2. N-(1-Benzoyl-1H-indol-6-yl)-5-chloro-2-hydroxybenzamide (5b). White powder, 35.45% yield, m.p: 171.5–172.4 °C. ^{1}H NMR (500 MHz, DMSO-d_6) δ (ppm): 12.01 (s, 1H), 10.60 (s, 1H), 8.84 (s, 1H), 8.06 (d, J = 2.4 Hz, 1H), 7.77 (d, J = 7.3 Hz, 2H), 7.71–7.63 (m, 3H), 7.60 (t, J = 7.5 Hz, 2H), 7.47 (dd, J = 8.8, 2.5 Hz, 1H), 7.34 (d, J = 3.7 Hz, 1H), 7.03 (d, J = 8.8 Hz, 1H), 6.73 (d, J = 3.6 Hz, 1H). ^{13}C NMR (126 MHz, DMSO-d_6) δ (ppm): 168.26, 165.25, 157.28, 135.48, 135.09, 134.01, 133.08, 131.99, 128.91, 128.68, 128.25, 128.23, 127.23, 122.69, 120.83, 119.13, 117.97, 108.83, 108.29. ESI-MS m/z: 391.0 $(M + H)^+$.

4.2.3.3. N-(1-Benzoyl-1H-indazol-4-yl)-5-chloro-2-hydroxybenzamide (5c). White powder, 42.54% yield, m.p: 222.5–223.3 °C. ^{1}H NMR (500 MHz, DMSO-d_6) δ (ppm): 10.91 (s, 1H), 8.53 (s, 1H), 8.25 (d, J = 8.3 Hz, 1H), 8.02–7.96 (m, 3H), 7.90 (d, J = 7.8 Hz, 1H), 7.73–7.64 (m, 2H), 7.57 (t, J = 7.6 Hz, 2H), 7.50 (dd, J = 8.8, 2.7 Hz, 1H), 7.07 (d, J = 8.8 Hz, 1H). ^{13}C NMR (126 MHz, DMSO-d_6) δ (ppm): 167.92, 164.82, 156.45, 140.23, 139.11, 133.16, 132.98, 132.26, 130.93, 130.60, 130.44, 128.86, 127.98, 122.90, 119.90, 119.34, 119.09, 117.24, 111.51. ESI-MS m/z: 392.0 $(M + H)^+$.

4.2.3.4. N-(1-Bbenzoyl-1H-indazol-5-yl)-5-chloro-2-hydroxybenzamide (5d). Yellow powder, 54.23% yield, m.p: 225.3–226.5 °C. ^{1}H NMR (500 MHz, DMSO-d_6) δ (ppm): 11.83 (s, 1H), 10.68 (s, 1H), 8.56 (s, 1H), 8.42 (d, J = 9.3 Hz, 2H), 8.00 (d, J = 8.1 Hz, 3H), 7.88 (d, J = 8.9 Hz, 1H), 7.67 (t, J = 7.4 Hz, 1H), 7.57 (t, J = 7.6 Hz, 2H), 7.48 (dd, J = 8.8, 2.3 Hz, 1H), 7.04 (d, J = 8.8 Hz, 1H). ^{13}C NMR (126 MHz, DMSO-d_6) δ (ppm): 167.56, 165.17, 156.85, 141.17, 136.29, 135.09, 133.12, 132.96, 132.26, 130.74, 128.44, 127.99, 126.38, 123.74, 122.79, 119.62, 119.12, 115.36, 112.56. ESI-MS m/z: 392.0 $(M + H)^+$.

4.2.4. Synthesis of 1-(tetrahydro-2H-pyran-2-yl)-1H-indazol-4-amine (6)

To a solution of 5.0 mL (8.35 g, 59.7 mmol) of 3, 4-dihydropyran in dry THF (30 mL) was added 5.0 g (30.7 mmol) of 4-nitro-1*H*-indazole (**5**) and 60 mg (0.23 mmol) of p-TsOH. The resulting solution was stirred at room temperature for 12 h, and then quenched with H_2O (30 mL) and extracted with AcOEt (3 × 30 mL). The organic layers were dried over $MgSO_4$ and concentrated at reduced pressure. The residue (5.0 g) in dry THF (30 mL) was added 20% Pd/C (1.0 g) and stirred for 2 h under hydrogen atmosphere. The resulting mixture was filtered and the filtrate was concentrated under reduced pressure. The residue was purified by chromatography on silica gel to give compound **6** (4.79 g, 72.1%) as a white powder. ^{1}H NMR (500 MHz, $CDCl_3$) δ (ppm): 7.98 (s, 1H), 7.22–7.14 (m, 1H), 6.97 (d, J = 8.4 Hz, 1H), 6.38 (d, J = 7.4 Hz, 1H), 5.70–5.59 (m, 1H), 4.14–3.97 (m, 1H), 3.82–3.68 (m, 1H), 3.41 (s, 2H), 2.64–2.49 (m, 1H), 2.24–2.10 (m, 1H), 2.09–1.95 (m, 1H), 1.83–1.69 (m, 2H), 1.66–1.51 (m, 1H).

4.2.5. Synthesis of 2-(benzyloxy)-5-chlorobenzoic acid (7)

A solution of 5-chloro-2-hydroxybenzoic acid (**2**) (2.0 g, 11.6 mmol) in dry DMF (15 mL) was added K_2CO_3 (4.81 g, 34.8 mmol) portionwise, followed by benzyl chloride (1.33 mL, 34.8 mmol) at room temperature. The mixture was stirred at room temperature and monitored by thin layer chromatography (TLC). The resulting mixture was quenched with saturated NH_4Cl solution (10 mL), and the mixture was extracted with AcOEt (3 × 10 mL). The organic layers were washed by brine, dried over $MgSO_4$ and concentrated at reduced pressure. The residue was dissolved in a solution of THF-EtOH (1:1, 10 mL), 5 moL/L NaOH (5.0 mL) was then added slowly. The reaction solution was stirred for 12 h and concentrated at reduced pressure. The aqueous layer was then acidified with 10% HCl to pH 2–3. The precipitated product was filtered and washed with water (20 mL) to yield the desired compound **7** (2.74 g, 90.3%) as a white powder.

4.2.6. Synthesis of 2-(benzyloxy)-5-chloro-N-(1-(tetrahydro-2H-pyran-2-yl)-1H-indazol-4-yl) benzamide (8)

This compound was synthesized following a procedure described in preparing compounds **4a-4g**. Yellow powder, 67% yield, m.p: 212.1–213.4 °C. ^{1}H NMR (500 MHz, $CDCl_3$) δ (ppm): 10.14 (s, 1H), 8.35 (d, J = 2.0 Hz, 1H), 7.92 (d, J = 5.2 Hz, 1H), 7.56–7.39 (m, 6H), 7.33 (s, 2H), 7.20–7.03 (m, 2H), 5.67 (d, J = 6.1 Hz, 1H), 5.31 (s, 2H), 4.02 (d, J = 9.1 Hz, 1H), 3.73 (s, 1H), 2.50 (s, 1H), 2.14 (s, 1H), 2.08–1.93 (m, 1H), 1.76 (s, 3H).

4.2.7. Synthesis of 2-(benzyloxy)-5-chloro-N-(1H-indazol-4-yl) benzamide (9)

The solution of compound **8** (2.0 g, 4.34 mmol) in dry CH_2Cl_2 (20 mL) was added trifluoroacetic acid (TFA, 5 mL) slowly at room temperature. After stirring for 5 h, the reaction solution was concentrated at reduced pressure. The aqueous layer was then basified with saturated $NaHCO_3$ to pH = 7. The precipitated product was filtered and washed with water (20 mL) to yield the compound **9** (1.51 g, 92.3%) as a white powder. m.p: 242.2–423.7 °C. ^{1}H NMR (500 MHz, DMSO-d_6) δ (ppm): 13.08 (s, 1H), 10.38 (s, 1H), 7.84 (s, 1H), 7.77 (s, 2H), 7.60 (d, J = 8.9 Hz, 1H), 7.52 (s, 2H), 7.37 (d, J = 8.9 Hz, 1H), 7.34–7.22 (m, 5H), 5.30 (s, 2H).

4.2.8. General procedures for the synthesis of compounds 10a-10f

4.2.8.1. 2-(Benzyloxy)-5-chloro-N-{1-[4-(dimethylamino) benzoyl]-1H-indazol-4-yl}benzamide (10a). Yellow powder, 54.3% yield, m.p: 196.5–198.4 °C. ^{1}H NMR (500 MHz, $CDCl_3$) δ (ppm): 10.17 (s, 1H), 8.36 (s, 1H), 8.24 (d, J = 8.3 Hz, 1H), 8.12 (d, J = 8.6 Hz, 2H), 7.83 (d, J = 7.7 Hz, 1H), 7.53 (d, J = 6.5 Hz, 2H), 7.51–7.43 (m, 5H), 7.29 (s, 1H), 7.13 (d, J = 8.8 Hz, 1H), 6.84 (d, J = 8.1 Hz, 2H), 5.29 (s, 2H), 3.11 (s, 6H). ESI-MS m/z: 525.2 $(M + H)^+$.

4.2.8.2. 2-(Benzyloxy)-5-chloro-N-[1-(2,6-dichlorobenzoyl)-1H-indazol-4-yl]benzamide (10b). Yellow powder, 35.4% yield, m.p: 198.2–199.0 °C. ^{1}H NMR (500 MHz, DMSO-d_6) δ (ppm): 10.48 (s, 1H), 9.39 (s, 1H), 7.88 (d, J = 6.6 Hz, 1H), 7.75–7.66 (m, 4H), 7.60 (dd, J = 8.8, 2.3 Hz, 1H), 7.49 (d, J = 5.8 Hz, 2H), 7.39–7.32 (m, 3H), 7.26–7.19 (m, 3H), 5.24 (s, 2H). ESI-MS m/z: 550.1 $(M + H)^+$.

4.2.8.3. 2-(Benzyloxy)-5-chloro-N-[1-(furan-2-carbonyl)-1H-indazol-4-yl] benzamide (10c). Yellow powder, 25.4% yield, m.p: 212.1–213.3 °C. ^{1}H NMR (500 MHz, DMSO-d_6) δ (ppm): 10.63 (s, 1H), 8.29 (s, 1H), 8.19 (s, 1H), 8.16 (d, J = 8.3 Hz, 1H), 7.97 (d, J = 3.2 Hz, 1H), 7.95 (d, J = 8.0 Hz, 1H), 7.76 (s, 1H), 7.67–7.59 (m, 2H), 7.51 (d, J = 5.5 Hz, 2H), 7.37 (d, J = 8.8 Hz, 1H), 7.36–7.27 (m, 3H), 6.86 (d, J = 1.6 Hz, 1H), 5.28 (s, 2H). ESI-MS m/z: 472.2 $(M + H)^+$.

4.2.8.4. 2-(Benzyloxy)-5-chloro-N-[1-(3, 4, 5-trimethoxybenzoyl)-1H-indazol-4-yl] benzamide (10d). White powder, 47.6% yield, m.p: 197.1–198.5 °C. ^{1}H NMR (500 MHz, $CDCl_3$) δ (ppm): 10.18 (s, 1H), 8.37 (d, J = 2.7 Hz, 1H), 8.27 (d, J = 8.1 Hz, 1H), 7.70 (d, J = 7.7 Hz, 1H), 7.57–7.51 (m, 3H), 7.50 (d, J = 1.8 Hz, 1H), 7.48–7.43 (m, 4H), 7.41 (s, 2H), 7.15 (d, J = 8.9 Hz, 1H), 5.30 (s, 2H), 3.97 (s, 3H), 3.95 (s, 6H). ESI-MS m/z: 573.3 $(M + H)^+$.

4.2.8.5. 2-(Benzyloxy)-5-chloro-N-[1-(morpholine-4-carbonyl)-1H-indazol-4-yl] benzamide (10e). White powder, 78.4% yield, m.p: 201.5–202.5 °C. ^{1}H NMR (500 MHz, DMSO-d_6) δ (ppm): 10.52 (s, 1H), 8.09 (s, 1H), 7.86 (d, J = 7.6 Hz, 1H), 7.75 (d, J = 2.3 Hz, 1H), 7.68 (d, J = 8.3 Hz, 1H), 7.60 (dd, J = 8.8, 2.3 Hz, 1H), 7.52–7.46 (m, 3H), 7.37 (d, J = 8.9 Hz, 1H), 7.33–7.26 (m, 3H), 5.28 (s, 2H), 3.71 (s, 8H). ESI-MS m/z: 491.2 $(M + H)^+$.

4.2.8.6. 4-[2-(benzyloxy)-5-chlorobenzamido]-N-(4-methoxyphenyl)-1H-indazole-1-carboxamide (10f). White powder, 65.8% yield, m.p: 213.6–215.2 °C. ^{1}H NMR (500 MHz, DMSO-d_6) δ (ppm): 10.61 (s, 1H), 10.25 (s, 1H), 8.48 (s, 1H), 8.08 (d, J = 8.3 Hz, 1H), 7.88 (d, J = 7.7 Hz, 1H), 7.73 (d, J = 2.3 Hz, 1H), 7.67 (d, J = 8.9 Hz, 2H), 7.59 (dd, J = 8.8, 2.3 Hz, 1H), 7.56 (t, J = 8.1 Hz, 1H), 7.49 (s, 1H), 7.48 (s, 1H), 7.35 (d, J = 8.9 Hz, 1H), 7.32–7.24 (m, 3H), 6.95 (d, J = 8.9 Hz, 2H), 5.28 (s, 2H), 3.76 (s, 3H). ESI-MS m/z: 527.1 $(M + H)^+$.

4.2.9. General procedures for the synthesis of compounds 11a-11f

To a solution of compounds **10a-10f** (0.1 mmol) in dry THF (20 mL) was added 20% Pd/C (1.0 g) and stirred for 3–6 h under hydrogen atmosphere. The resulting mixture was filtered and the filtrate was concentrated under reduced pressure. The residue was purified by chromatography on silica gel to give title compounds **11a-11f**, respectively.

4.2.9.1. 5-Chloro-N-{1-[4-(dimethylamino) benzoyl]-1H-indazol-4-yl}-2-hydroxybenzamide (11a). Green powder, 78.2% yield, m.p: 267.2–267.8 °C. ^{1}H NMR (500 MHz, DMSO-d_6) δ (ppm): 10.99 (s, 1H), 8.48 (s, 1H), 8.18 (d, J = 8.3 Hz, 1H), 8.04 (d, J = 8.8 Hz, 2H), 8.00 (d, J = 2.1 Hz, 1H), 7.87 (d, J = 7.7 Hz, 1H), 7.63 (t, J = 8.0 Hz, 1H), 7.50 (dd, J = 8.7, 2.3 Hz, 1H), 7.12 (d, J = 8.8 Hz, 1H), 6.79 (d, J = 8.9 Hz, 2H), 3.05 (s, 6H). ESI-MS m/z: 435.0 $(M + H)^+$.

4.2.9.2. 5-Chloro-N-[1-(2,6-dichlorobenzoyl)-1H-indazol-4-yl]-2-hydroxybenzamide (11b). Yellow powder, 53.2% yield, m.p: 255.3–256.4 °C. ^{1}H NMR (500 MHz, DMSO-d_6) δ (ppm): 11.69 (s, 1H), 10.69 (s, 1H), 9.37 (s, 1H), 7.93 (d, J = 2.4 Hz, 1H), 7.74 (t, J = 3.9 Hz, 1H), 7.72–7.66 (m, 3H), 7.49 (dd, J = 8.8, 2.7 Hz, 1H), 7.41 (d, J = 4.2 Hz, 2H), 7.06 (d, J = 8.8 Hz, 1H). ^{13}C NMR (126 MHz, DMSO-d_6) δ (ppm): 164.72, 156.09, 151.92, 133.10, 132.86, 132.68, 131.25, 131.19, 131.10, 128.90, 128.34, 122.84, 122.38, 120.68, 118.92, 118.33, 114.65, 114.01. ESI-MS m/z: 460.9 $(M + H)^+$.

4.2.9.3. 5-Chloro-N-[1-(furan-2-carbonyl)-1H-indazol-4-yl]-2-hydroxybenzamide (11c). White powder, 45.6% yield, m.p: 278.0–279.8 °C. ^{1}H NMR (500 MHz, DMSO-d_6) δ (ppm): 11.33 (s, 1H), 8.58 (s, 1H), 8.20 (d, J = 8.4 Hz, 1H), 8.19 (s, 1H), 8.03–7.95 (m, 2H), 7.91 (d, J = 7.7 Hz, 1H), 7.66 (t, J = 8.0 Hz, 1H), 7.47 (dd, J = 8.8, 2.5 Hz, 1H), 7.11 (d, J = 8.8 Hz, 1H), 6.84 (dd, J = 3.4, 1.5 Hz, 1H). ^{13}C NMR (500 MHz, DMSO-d_6) δ (ppm): 164.80, 156.49, 155.94, 149.20, 139.71, 136.30, 133.14, 130.92, 130.64, 129.76, 128.91, 122.92, 122.59, 120.00, 119.10, 115.54, 113.87, 110.64, 55.24. ESI-MS m/z: 382.1 $(M + H)^+$.

4.2.9.4. 5-Chloro-2-hydroxy-N-(1-(3,4,5-trimethoxybenzoyl)-1H-indazol-4-yl)benzamide (11d). White powder, 67.2% yield, m.p: 190.2–191.2 °C. ^{1}H NMR (500 MHz, DMSO-d_6) δ (ppm): 11.84 (s, 1H), 10.92 (s, 1H), 8.54 (s, 1H), 8.21 (d, J = 8.3 Hz, 1H), 7.98 (s, 1H), 7.89 (d, J = 7.6 Hz, 1H), 7.69 (t, J = 8.0 Hz, 1H), 7.50 (d, J = 8.7 Hz, 1H), 7.36 (s, 2H), 7.07 (d, J = 8.8 Hz, 1H), 3.84 (s, 6H), 3.79 (s, 3H). ^{13}C NMR (126 MHz, DMSO-d_6) δ (ppm): 167.11, 164.80, 156.53, 152.18, 141.20, 140.36, 138.95, 133.14, 130.95, 130.33, 128.86, 127.77, 122.85, 119.85, 119.30, 119.09, 117.08, 111.41, 108.83, 60.18, 56.14. ESI-MS m/z: 482.2 $(M + H)^+$.

4.2.9.5. 5-Chloro-2-hydroxy-N-[1-(morpholine-4-carbonyl)-1H-indazol-4-yl]benzamide (11e). White powder, 67.4% yield, m.p: 216.7–217.8 °C. ^{1}H NMR (500 MHz, DMSO-d_6) δ (ppm): 11.88 (s, 1H), 10.84 (d, J = 7.4 Hz, 1H), 8.39 (d, J = 7.9 Hz, 1H), 7.99 (d, J = 7.5 Hz, 1H), 7.76 (s, 2H), 7.62–7.41 (m, 2H), 7.16–7.01 (m, 1H), 3.73 (s, 8H). ^{13}C NMR (126 MHz, DMSO-d_6) δ (ppm): 164.68, 156.43, 151.57, 140.99, 135.64, 133.11, 130.59, 128.97, 128.86, 122.92, 119.88, 119.08, 118.26, 115.12, 110.23, 66.03. ESI-MS m/z: 401.1 $(M + H)^+$.

4.2.9.6. 4-(5-Chloro-2-hydroxybenzamido)-N-(4-methoxyphenyl)-1H-indazole-1-carboxamide (11f). White powder, 74.5% yield, m.p: 231.4–232.5 °C. ^{1}H NMR (500 MHz, DMSO-d_6) δ (ppm): 11.78 (s, 1H), 10.87 (s, 1H), 10.29 (s, 1H), 8.50 (s, 1H), 8.14 (d, J = 8.4 Hz, 1H), 7.99 (d, J = 2.5 Hz, 1H), 7.81 (d, J = 7.6 Hz, 1H), 7.68 (d, J = 8.9 Hz, 2H), 7.60 (t, J = 8.0 Hz, 1H), 7.50 (dd, J = 8.8, 2.6 Hz, 1H), 7.07 (d, J = 8.8 Hz, 1H), 6.95 (d, J = 9.0 Hz, 2H), 3.76 (s, 3H). ^{13}C NMR (126 MHz, DMSO-d_6) δ (ppm): 164.76, 155.98, 148.85, 144.57, 140.22, 139.47, 133.04, 131.40, 130.65, 128.90, 123.56, 122.23, 119.91, 119.44, 118.89, 116.81, 112.81, 111.04. ESI-MS m/z: 436.4 $(M + H)^+$.

4.2.10. General procedures for the synthesis of compounds 14a-14d and 15a-15d

The key intermediates (**12a-12d** and its respective analogs **13a-13d**) were synthesized from compound **9** following a procedure described in preparing compounds **10a-10f**. The target compounds **14a-14d** and its respective analogs **15a-15d** were synthesized following a procedure described in preparing compounds **11a-11f**.

4.2.10.1. Methyl 3-(4-(5-chloro-2-hydroxybenzamido)-1H-indazol-1-yl) propanoate (14a). Yellow powder, 78.2% yield, m.p: 170.6–172.3 °C. ^{1}H NMR (500 MHz, DMSO-d_6) δ (ppm): 12.02 (s, 1H), 10.77 (s, 1H), 8.09 (s, 1H), 7.99 (d, J = 2.5 Hz, 1H), 7.72 (d, J = 7.4 Hz, 1H), 7.51–7.47 (m, 2H), 7.40 (t, J = 7.9 Hz, 1H), 7.08 (d, J = 8.8 Hz, 1H), 4.64 (t, J = 6.6 Hz, 2H), 3.55 (s, 3H), 2.95 (t, J = 6.6 Hz, 2H). ^{13}C NMR (126 MHz, DMSO-d_6) δ (ppm): 171.17, 164.06, 156.14, 140.21, 133.02, 130.90, 130.30, 129.02, 126.76, 123.07, 120.00, 119.07, 117.00, 111.89, 106.20, 51.45, 43.94, 33.67. ESI-MS m/z: 374.1 $(M + H)^+$.

4.2.10.2. 5-Chloro-2-hydroxy-N-[1-(2-hydroxyethyl)-1H-indazol-4-yl]benzamide (14b). White powder, 89.2% yield, m.p: 221.6–223.5 °C. ^{1}H NMR (500 MHz, DMSO-d_6) δ (ppm): 12.04 (s, 1H), 10.79 (s, 1H), 8.08 (s, 1H), 8.00 (d, J = 2.6 Hz, 1H), 7.71 (d, J = 7.4 Hz, 1H), 7.50 (dd, J = 8.8, 2.7 Hz, 1H), 7.46 (d, J = 8.4 Hz, 1H), 7.37 (t, J = 7.9 Hz, 1H), 7.08 (d, J = 8.8 Hz, 1H), 4.86 (s, 1H), 4.45 (t, J = 5.6 Hz, 2H), 3.82 (s, 2H). ^{13}C NMR (126 MHz, $CDCl_3$) δ (ppm): 161.94, 155.27, 134.44, 133.12, 132.64, 131.10, 129.86, 129.52, 128.94, 127.80, 127.59, 123.20, 114.36, 111.61, 105.05, 72.63, 61.81, 50.38. ESI-MS m/z: 333.2 $(M + H)^+$.

4.2.10.3. 5-Chloro-N-[1-(2-(dimethylamino)-2-oxoethyl)-1H-indazol-4-yl]-2-hydroxybenzamide (14c). White powder, 78.2% yield, m.p: 245.3–246.2 °C. ^{1}H NMR (500 MHz, DMSO-d_6) δ (ppm): 12.02 (s, 1H), 10.79 (s, 1H), 8.09 (s, 1H), 8.01 (s, 1H), 7.70 (s, 1H), 7.50 (d, J = 8.4 Hz, 1H), 7.36 (s, 2H), 7.08 (d, J = 8.4 Hz, 1H), 5.42 (s, 2H), 3.11 (s, 3H), 2.85 (s, 3H). ^{13}C NMR (126 MHz, DMSO-d_6) δ (ppm): 166.46, 164.08, 156.21, 141.31, 133.03, 130.76, 130.21, 129.01, 126.53, 123.05, 119.98, 119.09, 117.17, 111.77, 106.58, 50.20, 35.96, 35.19. ESI-MS m/z: 373.1 $(M + H)^+$.

4.2.10.4. 4-(5-Chloro-2-hydroxybenzamido)-N,N-dimethyl-1H-indazole-1-carboxamide (14d). White powder, 45.3% yield, m.p: 248.4–249.3 °C. ^{1}H NMR (500 MHz, DMSO-d_6) δ (ppm): 11.89 (s, 1H), 10.82 (s, 1H), 8.36 (s, 1H), 7.99 (s, 1H), 7.75 (s, 1H), 7.72 (s, 1H), 7.51 (s, 2H), 7.07 (s, 1H), 3.15 (s, 6H). ^{13}C NMR (126 MHz, DMSO-d_6) δ (ppm): 164.64, 156.41, 152.58, 140.91, 135.07, 133.10, 130.51, 128.87, 128.72, 122.93, 119.87, 119.07, 118.13, 114.86, 110.13. ESI-MS m/z: 359.1 $(M + H)^+$.

4.2.10.5. Methyl 3-[4-(5-chloro-2-hydroxybenzamido)-2H-indazol-2-yl] propanoate (15a). Yellow powder, 65.4% yield, m.p: 99.8–101.2 °C. ^{1}H NMR (500 MHz, DMSO-d_6) δ (ppm): 12.02 (s, 1H), 10.64 (s, 1H), 8.40 (s, 1H), 8.00 (d, J = 2.2 Hz, 1H), 7.54 (d, J = 7.1 Hz, 1H), 7.50 (dd, J = 8.7, 2.4 Hz, 1H), 7.42 (d, J = 8.5 Hz, 1H), 7.25 (t, J = 7.9 Hz, 1H), 7.07 (d, J = 8.8 Hz, 1H), 4.68 (t, J = 6.3 Hz, 2H), 3.59 (s, 3H), 3.07 (t, J = 6.4 Hz, 2H). ^{13}C NMR (126 MHz, DMSO-d_6) δ (ppm): 171.01, 164.26, 156.46, 148.88, 133.05, 129.95, 128.84, 125.85, 123.04, 122.97, 119.77, 119.11, 116.26, 113.69, 112.18, 51.59, 48.47, 34.03. ESI-MS m/z: 374.1 $(M + H)^+$.

4.2.10.6. 5-Chloro-2-hydroxy-N-[2-(2-hydroxyethyl)-2H-indazol-4-yl]benzamide (15b). White powder, 78.2% yield, m.p: 175.6–176.9 °C. ^{1}H NMR (500 MHz, DMSO-d_6) δ (ppm): 12.00 (s, 1H), 10.68 (s, 1H), 8.38 (s, 1H), 8.00 (d, J = 2.6 Hz, 1H), 7.57 (d, J = 7.2 Hz, 1H), 7.49 (dd, J = 8.8, 2.7 Hz, 1H), 7.42 (d, J = 8.6 Hz, 1H), 7.28–7.20 (m, 1H), 7.07 (d, J = 8.8 Hz, 1H), 5.00 (s, 1H), 4.47 (t, J = 5.3 Hz, 2H), 3.88 (s, 2H). ^{13}C NMR (126 MHz, DMSO-d_6) δ (ppm): 164.18, 156.46, 148.79, 132.98, 129.92, 128.85, 125.61, 123.06, 122.90, 119.81, 119.10, 116.24, 113.52, 111.82, 60.05, 55.75. ESI-MS m/z: 332.1 $(M + H)^+$.

4.2.10.7. 5-Chloro-N-{2-[2-(dimethylamino)-2-oxoethyl]-2H-indazol-4-yl}-2-hydroxybenzamide (15c). White powder, 67.4% yield, m.p: 262.5–263.4 °C. ^{1}H NMR (500 MHz, DMSO-d_6) δ (ppm): 12.06 (s, 1H), 10.70 (s, 1H), 8.34 (s, 1H), 8.01 (s, 1H), 7.57 (d, J = 7.1 Hz, 1H), 7.50 (d, J = 8.9 Hz, 1H), 7.41 (d, J = 8.7 Hz, 1H), 7.25 (t, J = 8.0 Hz, 1H), 7.07 (d, J = 8.7 Hz, 1H), 5.48 (s, 2H), 3.09 (s, 3H), 2.87 (s, 3H). ^{13}C NMR (126 MHz, DMSO-d_6) δ (ppm): 166.02, 164.21, 156.46, 148.61, 133.02, 129.95, 128.83, 125.76, 124.28, 122.97, 119.72, 119.11, 116.53, 113.60, 111.98, 54.20, 36.07, 35.24. ESI-MS m/z: 373.1 $(M + H)^+$.

4.2.10.8. 4-(5-Chloro-2-hydroxybenzamido)-N, N-dimethyl-2H-indazole-2-carboxamide (15d). White powder, 74.9% yield, m.p: 112.7–113.4 °C. ^{1}H NMR (500 MHz, DMSO-d_6) δ (ppm): 11.84 (s, 1H), 10.67 (s, 1H), 8.84 (s, 1H), 7.94 (d, J = 2.5 Hz, 1H), 7.70 (d, J = 7.1 Hz, 1H), 7.51–7.43 (m, 2H), 7.40–7.33 (m, 1H), 7.05 (d, J = 8.8 Hz, 1H), 3.17 (s, 6H). ^{13}C NMR (126 MHz, DMSO-d_6) δ (ppm): 164.36, 156.11, 151.84, 149.10, 132.91, 130.82, 128.93, 128.61, 124.28, 122.95, 120.39, 118.99, 115.78, 114.07, 112.61. ESI-MS m/z: 359.1 $(M + H)^+$.

4.2.11. General procedures for the synthesis of compounds 16a and 17a

To a stirred solution of **14a** and **15a** (0.1 mmol) in MeOH (20 mL) was added 10% NaOH (10 mL) slowly. The resulting solution was stirred for 3 h and then quenched by water, the solution was removed MeOH in vacuo, and the solution was acidated to pH = 2–3 with 6 N HCl. The precipitated product was collected by vacuum filtration, and the remaining dissolved product was extracted with EtOAc (2 × 20 mL). The precipitate was dissolved in THF, and its solution was combined with organic layers from the extractions. Dried over $MgSO_4$, filtration, concentration in vacuo, and crystallization with THF/EtOAc/hexane afforded desired compounds **16a** and **17a**, respectively.

4.2.11.1. 3-[4-(5-Chloro-2-hydroxybenzamido)-1H-indazol-1-yl] propanoic acid (16a). Yellow powder, 69.4% yield, m.p: 196.3–198.2 °C. ^{1}H NMR (500 MHz, DMSO-d_6) δ (ppm): 12.26 (s, 1H), 10.97 (s, 1H), 8.09 (s, 1H), 7.98 (d, J = 2.6 Hz, 1H), 7.75 (d, J = 7.4 Hz, 1H), 7.51–7.45 (m, 2H), 7.39 (t, J = 8.0 Hz, 1H), 7.07 (d, J = 8.8 Hz, 1H), 4.60 (t, J = 6.7 Hz, 2H), 2.87 (t, J = 6.7 Hz, 2H). ^{13}C NMR (126 MHz, DMSO-d_6) δ (ppm): 167.52, 165.17, 156.85, 141.11, 136.30, 135.04, 133.09, 132.93, 132.22, 130.68, 128.40, 127.95, 126.35, 123.75, 122.77, 119.54, 119.10, 115.31, 112.59, 39.96. ESI-MS m/z: 360.1 $(M + H)^+$.

4.2.11.2. 3-[4-(5-Chloro-2-hydroxybenzamido)-2H-indazol-2-yl] propanoic acid (17a). Yellow powder, 78.2% yield, m.p: 105.2–107.1 °C. ^{1}H NMR (500 MHz, DMSO-d_6) δ (ppm): 10.73 (s, 1H), 8.39 (s, 1H), 7.99 (d, J = 2.7 Hz, 1H), 7.55 (d, J = 7.3 Hz, 1H), 7.48 (dd,

J = 8.8, 2.7 Hz, 1H), 7.41 (d, J = 8.6 Hz, 1H), 7.24 (dd, J = 8.6, 7.4 Hz, 1H), 7.06 (d, J = 8.8 Hz, 1H), 4.64 (t, J = 6.6 Hz, 2H), 2.97 (t, J = 6.6 Hz, 2H). ^{13}C NMR (126 MHz, DMSO-d_6) δ (ppm): 171.99, 164.28, 156.72, 148.86, 133.03, 130.02, 129.65, 128.86, 125.85, 122.94, 122.80, 119.80, 119.20, 116.22, 113.59, 112.02, 48.71, 34.39. ESI-MS m/z: 360.0 $(M + H)^+$.

4.3. Cell culture

MG63, U2OS, and MIHA cells were presented by Sun Yat-sen University. hFOB 1.19 cells were obtained from the Cell Resource Center, Shanghai Academy of Biological Sciences, Chinese Academy of Sciences. MG 63, U2OS, and MIHA cells were cultured at 37 °C under 5% CO_2. DMEM (Sigma) supplemented with 10% fetal calf serum (PPA) and 100 U/mL penicillin and streptomycin (HyClone), and hFOB 1.19 was cultured with DMEM/F12 (PM150312) +0.3 mg/mL G418 (PB180125) + 10% FBS(164210-500)+1%P/S(PB180120), other conditions are the same as the previous three cells.

4.4. Cell viability assay

The 3-(4, 5-dimethylthiazol-2-yl)-2, 5-diphenyltetrazolium bromide (MTT) assay was used to assess cell viability. Cells (5000 cells/well in 96-well plates) were incubated at 37 °C for 6 h and then treated with synthetic compounds at a concentration of 40 μM for 48 h. Subsequently, MTT was added to the cells at a concentration of 0.5 mg/mL per well for another 4 h. The reaction product formazan was dissolved in 100 μL DMSO after discarding the culture medium. The cell viability was determined by reading the absorbance at 490 nm with the American thermoelectric Thermo Fisher Multiskan FC automatic microplate reader. The result is expressed as the mean ± standard deviation of three measurements (n = 3).

4.5. Long-term proliferation studies

MG63 and U2OS cells (2.0×10^5) were seeded in a 6-well plate. After 6 h, **5d** was added to a final concentration of 0, 5.0, 10.0, or 20.0 μM. During the proliferation process, the cell numbers in each well were counted using a cytometer (Countstar, China). Then, the cells (2.0×10^5) were transfer into a 6-well until the cells were less than 2.0×10^5. $2^{PDs} = M/N$ (PDs: population doublings, M: number of every count cells, N: number of cells implanted).

4.6. Western blot

MG63, U2OS cells (2.0×10^5) were seeded in a 6-well plate. After 6 h, **5d** was added to a final concentration of 0, 5.0, 10.0, or 20.0 μM for 48 h. Subsequently, the treated cells were lysed and boiled for 10 min. Proteins were separated by SDS-PAGE, transferred to a PVDF membrane, and detected with relevant antibodies against FAK (CST), phospho-FAK (CST), RPA (CST), γH2AX (CST), or GAPDH (CST).

4.7. Cell cycle distribution analysis

MG63 and U2OS cells were cultured in the absence or presence of 0, 5.0, 10.0, and 20.0 μM texted compound for 48 h. The cells were trypsinized, washed, and stained with propidium iodide before the cell cycle distribution was assessed on a flow cytometer (BD FACSCalibur, BD Biosciences).

4.8. Annexin V/PI apoptosis assay

MG63 and U2OS cells were seeded in a 6 cm^2 dish at a density of 3.0×10^5 cells per dish and incubated at 37 °C for 6 h until cells attached to the dish. 5d with final concentration of 0, 5.0, 10.0, and 20.0 μM was added to the medium. After 72 h, cells were harvested for Anexin V/PI apoptosis assay. The assay was performed following the protocol provided by the Annexin V/PI apoptosis Kit (Sigma), and the cells were assessed on a flow cytometer (BD FACSCalibur, BD Biosciences).

4.9. Comet assay

The comet assay was used to detect the DNA damage. In short, treated cells were mixed with 0.5% low-melting temperature agarose and layered on slides pre-coated by 1.5% normal agarose. Then, the slides were lysed in 2.5 M NaCl, 100 mM EDTA, 10 mM Tris (pH 8.0), 0.5% Triton X-100, 3% DMSO, and 1% N-lauroylsarcosine. The lysed cells underwent electrophoresis in 300 mM sodium acetate, 100 mM Tris-HCl, and 1% DMSO. The slides were then mounted with PI solution and visualized via fluorescence microscopy (Nikon Ti microscope). Analysis was performed with CASP. Over 200 cells from each group were randomly chosen from three independent experiments.

4.10. Wound healing migration assay

In order to explore the effect of the compound on cell migration ability, MG63 and U2OS cells were treated with 5d for 48 h. The cells were seeded in a 6-well plate and grown to confluence in growth medium. Using a sterile pipette tip, a scratch about 1 mm wide was created on the cell layer. Pictures of the plate were taken immediately after scratching at the same position (0 h) and again at 24, 48, 72, and 96 h. The scratched area was measured at each time point. The migration area inhibition rate was 100%-(A0h-A24h)/A0h × 100% (taking 24 h as an example). All experiments were performed in triplicate.

4.11. Cell adhesion assay

At room temperature, we coated a 96-well plate with 2.5 μg/mL human fibronectin in PBS (Millipore, CA). Then, the treated cells were seeded into serum-free medium at a density of 3.5×10^4 cells/well. The cells were cultured at 37 °C for 30 min under 5% CO_2. The cells treated with 0.1% DMSO were used as the control group. The medium was gently removed, and the cells were fixed with 4% paraformaldehyde. Attached cells were stained with crystal violet at room temperature for 5 min. After dissolving the crystal violet in 100 μL DMSO, the absorbance was measured at 560 nm. Use the following formula to calculate the relative number of cells attached to the extracellular matrix: average of treated cells OD/average OD control unit. The relative number of cells attached to the extracellular matrix was calculated using the following equation: (mean OD of treated cells/mean OD of control cells) × 100%.

4.12. Transwell assay

Treated cells were digested, resuspended, and diluted with serum-free media to a concentration of 1×10^5/100 μL. Transwell chambers were inserted into a 24-well plate. Subsequently, 600 μL of 10% FBS was added into the lower chamber. After 100 μL of prepared cell suspension was pipetted from each group into the upper chamber, the 24-well plate was cultured in a 37 °C incubator. After 24 h, the fluid and cells in the chamber were discarded, and the cells were washed three times with pre-warmed PBS. The cells were fixed with 4% paraformaldehyde for 15 min at room temperature, and, subsequently, the cells on the chamber membrane were washed three times with dd water (5 min each time). The cells

were stained with crystal violet for 5 min. The chamber was rinsed with dd water and 30% glacial acetic acid to dissolve the crystal violet, and t the absorbance was measured at 560 nm. Cell migration rate: average of treated cells OD/average OD control unit) × 100%.

4.13. Mitochondrial membrane potential

In order to explore the changes in cell mitochondrial membrane potential after treatment, JC-1 (5, 5′, 6, 6′-tetrachloro-1, 1′, 3, 3′-tetraethylbenzimi-dazolylcarbocyanine iodide) staining was performed. Energized mitochondria were differentiated from de-energized mitochondria by enumerating the normally green fluorescence dye (J-monomers), and its conversion to red fluorescence (J-aggregates) upon accumulation in energized mitochondria was used (Abcam, Cambridge, MA). The higher red to green fluorescence intensity ratio indicated the increased mitochondrial membrane potential.

4.14. RNA library construction and sequencing

U2OS and MG63 cells were treated for 48 h with 10 μM 5d, and RNA was sequenced. The total RNA was extracted by TRIzol reagent (Invitrogen, CA, USA). Then, paired-end sequencing was performed on an Illumina HiSeq 4000 at LC-BIO Technologies (Hangzhou) Co., LTD., following the vendor's recommended protocol.

4.15. Statistical analysis

All data were analyzed by Graphpad Prism 7.0 and SPSS 19.0. The means of multiple groups were compared by one-way analysis of variance, and the means of two groups were compared with the independent samples *t*-test. Values are expressed as the average ± SD of three independent experiments. *p < 0.05, **p < 0.01; ***p < 0.001.

Declaration of competing interest

The authors declare that they have no known competing financial interests or personal relationships that could have appeared to influence the work reported in this paper.

Acknowledgement

We acknowledge the support of the National Natural Science Funding of China (81973168, 81773579, and 21701194), Wenzhou Public Welfare Science and Technology Project (2018Y0465 and Y20180177), and Wenzhou Medical University Talent Start-up Fund (QTJ17022) for the financial support. We thank LetPub (www.letpub.com) for its linguistic assistance during the preparation of this manuscript.

Appendix A. Supplementary data

Supplementary data to this article can be found online at https://doi.org/10.1016/j.ejmech.2021.113203.

References

[1] L. Mirabello, R. Troisi, Osteosarcoma incidence and survival rates from 1973 to 2004: data from the surveillance, epidemiology, and end results program, Cancer 115 (2009) 1531–1543.
[2] L. Kager, A. Zoubek, M. Dominkus, S. Lang, N. Bodmer, G. Jundt, Osteosarcoma in very young children: experience of the cooperative osteosarcoma study group, Cancer 116 (2010) 5316–5324.
[3] L. Kelley, M. Schlegel, S. Hecker-Nolting, M. Kevric, B. Haller, C. Rössig, et al., Pathological fracture and prognosis of high-grade osteosarcoma of the extremities: an analysis of 2,847 consecutive cooperative osteosarcoma study group (COSS) patients, J. Clin. Oncol. 38 (2020) 823–833.
[4] M. Isakoff, S. Bielack, P. Meltzer, Osteosarcoma: current treatment and a collaborative pathway to success, J. Clin. Oncol. 33 (2015) 3029–3035.
[5] R. Grimer, Surgical options for children with osteosarcoma, Lancet Oncol. 6 (2005) 85–92.
[6] U. Dirksen, B. Brennan, M. Le Deley, N. Cozic, H. Berg, V. Bhadri, et al., High-dose chemotherapy compared with standard chemotherapy and lung radiation in ewing sarcoma with pulmonary metastases: results of the European ewing tumour working initiative of national groups, 99 trial and EWING 2008, J. Clin. Oncol. 37 (2019) 3192–3202.
[7] K. Berner, K. Hall, O. Monge, H. Weedon-Fekjær, O. Zaikova, Prognostic Factors and Treatment Results of High-Grade Osteosarcoma in norway: a Scope beyond the "classical" Patient, Hindawi Publishing Corporation, 2015, 516843, 2015.
[8] J. Whelan, R. Jinks, A. McTiernan, M. Sydes, J. Hook, L. Trani, et al., Survival from high-grade localised extremity osteosarcoma: combined results and prognostic factors from three European Osteosarcoma Intergroup randomised controlled trials, Ann. Oncol. 23 (2012) 1607–1616.
[9] M. Heng, A. Gupta, P. Chung, J. Healey, M. Vaynrub, P. Rose, et al., The role of chemotherapy and radiotherapy in localized extraskeletal osteosarcoma, Eur. J. Canc. 125 (2020) 130–141.
[10] K. Janeway, Grier, Sequelae of osteosarcoma medical therapy: a review of rare acute toxicities and late effects, Lancet Oncol. 11 (2010) 670–678.
[11] S. Bielack, B. Kempf-Bielack, G. Delling, G. Exner, S. Flege, K. Helmke, et al., Prognostic factors in high-grade osteosarcoma of the extremities or trunk: an analysis of 1,702 patients treated on neoadjuvant cooperative osteosarcoma study group protocols, J. Clin. Oncol. 20 (2002) 776–790.
[12] A. Sarmento-Ribeiro, A. Scorilas, A. Gonçalves, T. Efferth, The emergence of drug resistance to targeted cancer therapies: clinical evidence, Drug Resist. Updates 47 (2019), 100646.
[13] A. Tanaka, S. Muto, K. Jung, A. Itai, Topical application with a new NF-kappaB inhibitor improves atopic dermatitis in NC/NgaTnd mice, J. Invest. Dermatol. 127 (2007) 855–863.
[14] A. Tanaka, M. Konno, S. Muto, N. Kambe, E. Morii, T. Nakahata, et al., A novel NF-kappaB inhibitor, IMD-0354, suppresses neoplastic proliferation of human mast cells with constitutively activated c-kit receptors, Blood 105 (2005) 2324–2331.
[15] J. Suzuki, M. Ogawa, S. Muto, A. Itai, M. Isobe, Y. Hirata, Novel IkB kinase inhibitors for treatment of nuclear factor-kB-related diseases, Expet Opin. Invest. Drugs 20 (2011) 395–405.
[16] M. Kanduri, G. Tobin, K. Nilsson, Rosenquist, The novel NF-κB inhibitor IMD-0354 induces apoptosis in chronic lymphocytic leukemia, Blood Canc. J., 2044-5385/11.
[17] A. Tanaka, S. Muto, M. Konno, A. Itai, Matsuda, A new IkappaB kinase beta inhibitor prevents human breast cancer progression through negative regulation of cell cycle transition, Canc. Res. 66 (2006) 419–426.
[18] A. Taniyama, Y. Terui, Y. Mishima, R. Kuniyoshi, K. Kojima, S. Muto, et al., Antitumor effect of IKKβ inhibitor IMD-0354 on bortezomib-resistant multiple myeloma cells, Mol. Canc. Therapeut. 6 (2007) 3393S, 3393S.
[19] Y. Cui, Z. Lu, L. Bai, Z. Shi, W. Zhao, beta-Carotene induces apoptosis and up-regulates peroxisome proliferator-activated receptor gamma expression and reactive oxygen species production in MCF-7 cancer cells, Eur. J. Canc. 43 (2007) 2590–2601.
[20] Y. Jiang, K. Zhang, S. Gao, G. Wang, J. Huang, J. Wang, Discovery of potent c-MET inhibitors with new scaffold having different quinazoline, pyridine and tetrahydro-pyridothienopyrimidine headgroups, Molecules (2016) 21.
[21] P. Lelieveld, R. Middeldorp, L. Putten, Effectiveness of P-aminobenzoyl-O-phenylenediamine (Goe 1734) against mouse, rat, and human tumour cells, Cancer Chemother, Pharmacol 5 (1985) 88–90.
[22] Q. Zhang, Y. Teng, Y. Yuan, T. Ruan, Q. Wang, X. Gao, et al., Synthesis and cytotoxic studies of novel 5-phenylisatin derivatives and their anti-migration and anti-angiogenic evaluation, Eur. J. Med. Chem. 156 (2018) 800–814.
[23] A. Elkamhawy, N. Kim, A. Hassan, J. Park, J. Yang, K. Oh, et al., Design, synthesis and biological evaluation of novel thiazolidinedione derivatives as irreversible allosteric IKK-β modulators, Eur. J. Med. Chem. 157 (2018) 691–704.
[24] L. Chen, W. Fu, C. Feng, R. Qu, L. Tong, L. Zheng, et al., Structure-based design and synthesis of 2,4-diaminopyrimidines as EGFR L858R/T790M selective inhibitors for NSCLC, Eur. J. Med. Chem. 140 (2017) 510–527.
[25] J. Kerns, J. Busch-Petersen, W. Fu, J. Boehm, H. Nie, M. Muratore, et al., 3,5-Disubstituted-indole-7-carboxamides as IKKβ inhibitors: optimization of oral activity via the C3 substituent, ACS Med. Chem. Lett. 9 (2018) 1164–1169.
[26] M. Zhang, X. Fang, C. Wang, Y. Hua, C. Huang, M. Wang, et al., Design and synthesis of 1H-indazole-3-carboxamide derivatives as potent and selective PAK1 inhibitors with anti-tumour migration and invasion activities, Eur. J. Med. Chem. 203 (2020) 112517.
[27] K. Czaja, J. Kujawski, P. Śliwa, R. Kurczab, R. Kujawski, A. Stodolna, et al., Theoretical investigations on interactions of arylsulphonyl indazole derivatives as potential ligands of VEGFR2 kinase, Int. J. Mol. Sci. 21 (2020).
[28] J. Liu, Y. Wen, L. Gao, L. Gao, F. He, J. Zhou, et al., HDesign, synthesis and biological evaluation of novel 1-1,2,4-triazole, benzothiazole and indazole-based derivatives as potent FGFR1 inhibitors fragment-based virtual screening, J. Enzym. Inhib. Med. Chem. 35 (2020) 72–84.
[29] I. Denya, S. Malan, J. Joubert, Indazole derivatives and their therapeutic

applications: a patent review (2013-2017), Expert Opin. Ther. Pat. 28 (2018) 441–453.
[30] E. Abdelsalam, W. Zaghary, K. Amin, N. Abou Taleb, A. Mekawey, W. Eldehna, et al., Synthesis and in vitro anticancer evaluation of some fused indazoles, quinazolines and quinolines as potential EGFR inhibitors, Bioorg. Chem. 89 (2019), 102985.
[31] S. Kim, D. Ko, Y. Lee, S. Jang, Y. Lee, I. Lee, et al., Anti-cancer activity of the novel 2-hydroxydiarylamide derivatives IMD-0354 and KRT1853 through suppression of cancer cell invasion, proliferation, and survival mediated by, TMPRSS4 9 (2019) 10003.
[32] A. Lennikov, P. Mirabelli, A. Mukwaya, M. Schaupper, M. Thangavelu, M. Lachota, et al., Selective IKK2 inhibitor IMD0354 disrupts NF-κB signaling to suppress corneal inflammation and angiogenesis, Sci. Rep. 21 (2018) 267–285.
[33] J. Robert-Paganin, O. Pylypenko, C. Kikuti, H. Sweeney, A. Houdusse, Force generation by myosin motors: a structural perspective, Chem. Rev. 120 (2020) 5–35.
[34] J. Hammer, J. Wang, M. Saeed, A. Pedrosa, Origin, organization, dynamics, and function of actin and actomyosin networks at the T cell immunological synapse, Annu. Rev. Immunol. 37 (2019) 201–224.
[35] P. Chaudhuri, B. Low, C. Lim, Mechanobiology of tumor growth, Chem. Rev. 118 (2018) 6499–6515.
[36] F. Sulzmaier, C. Jean, Schlaepfer, FAK in cancer: mechanistic findings and clinical applications, Nat. Rev. Canc. 14 (2014) 598–610.
[37] W. Long, P. Yi, L. Amazit, H. LaMarca, F. Ashcroft, R. Kumar, et al., SRC-3Delta4 mediates the interaction of EGFR with FAK to promote cell migration, Mol. Cell. 37 (2010) 321–332.
[38] J. Alanko, J. Ivaska, Endosomes: emerging platforms for integrin-mediated FAK signalling, Trends Cell Biol. 26 (2016) 391–398.
[39] L. Ding, X. Sun, Y. You, N. Liu, Expression of focal adhesion kinase and phosphorylated focal adhesion kinase in human gliomas is associated with unfavorable overall survival, Transl. Res. 156 (2010) 45–52.
[40] E. Paluch, I. Aspalter, Focal adhesion-independent cell migration, Annu. Rev. Cell Dev. Biol. 32 (2016) 469–490.
[41] V. Te Boekhorst, L. Preziosi, Plasticity of cell migration in vivo and in silico, Annu. Rev. Cell Dev. Biol. 32 (2016) 491–526.
[42] Y. Bae, K. Mui, B. Hsu, S. Liu, A. Cretu, Z. Razinia, et al., A FAK-Cas-Rac-lamellipodin signaling module transduces extracellular matrix stiffness into mechanosensitive cell cycling, Sci. Signal. 7 (2014) ra57.
[43] E. Klein, L. Yin, D. Kothapalli, P. Castagnino, F. Byfield, T. Xu, et al., Cell-cycle control by physiological matrix elasticity and in vivo tissue stiffening, Curr. Biol. 19 (2009) 1511–1518.
[44] F. Aboubakar Nana, M. Lecocq, M. Ladjemi, B. Detry, S. Dupasquier, O. Feron, et al., Therapeutic potential of focal adhesion kinase inhibition in small cell lung cancer, Mol. Canc. Therapeut. 18 (2019) 17–27.
[45] K. Banerjee, M. Keasey, V. Razskazovskiy, N. Visavadiya, C. Jia, T. Hagg, Reduced FAK-STAT3 signaling contributes to ER stress-induced mitochondrial dysfunction and death in endothelial cells, Cell. Signal. 36 (2017) 154–162.
[46] E. Kremneva, M. Kislin, X. Kang, L. Khiroug, Motility of astrocytic mitochondria is arrested by Ca2+-dependent interaction between mitochondria and actin filaments, Cell Calcium 53 (2013) 85–93.
[47] H. Kueh, T. Mitchison, Structural plasticity in actin and tubulin polymer dynamics, Science 325 (2009) 960–963.
[48] H. Inoue, K. Tani, Multimodal immunogenic cancer cell death as a consequence of anticancer cytotoxic treatments, Cell Death Differ. 21 (2014) 39–49.
[49] C. Lord, A. Ashworth, The DNA damage response and cancer therapy, Nature 481 (2012) 287–294.
[50] P. Bouwman, J. Jonkers, The effects of deregulated DNA damage signalling on cancer chemotherapy response and resistance, Nat. Rev. Canc. 12 (2012) 587–598.
[51] D. Cahill, B. Connor, J. Carney, Mechanisms of eukaryotic DNA double strand break repair, Front. Biosci. 11 (2006) 1958–1976.
[52] D. Lee, S. Acharya, M. Kwon, P. Drane, Y. Guan, G. Adelmant, et al., Dephosphorylation enables the recruitment of 53BP1 to double-strand DNA breaks, Mol. Cell 54 (2014) 512–525.
[53] D. Corujo, M. Buschbeck, Post-Translational modifications of H2A histone variants and their role in cancer, Cancers 10 (2018).
[54] K. Bhat, D. Cortez, RPA and RAD51: fork reversal, fork protection, and genome stability, Nat. Struct. Mol. Biol. 25 (2018) 446–453.
[55] A. Maréchal, L. Zou, RPA-coated single-stranded DNA as a platform for post-translational modifications in the DNA damage response, Cell Res. 25 (2015) 9–23.